https://ntrs.nasa.gov/search.jsp?R=19710003299 2018-07-26T08:42:57+00:00Z

General Disclaimer

One or more of the Following Statements may affect this Document

- This document has been reproduced from the best copy furnished by the organizational source. It is being released in the interest of making available as much information as possible.

- This document may contain data, which exceeds the sheet parameters. It was furnished in this condition by the organizational source and is the best copy available.

- This document may contain tone-on-tone or color graphs, charts and/or pictures, which have been reproduced in black and white.

- This document is paginated as submitted by the original source.

- Portions of this document are not fully legible due to the historical nature of some of the material. However, it is the best reproduction available from the original submission.

Produced by the NASA Center for Aerospace Information (CASI)

Col "Liquid Hydrogen"
Hy t

A Reproduced Copy

OF

Reproduced for NASA

by the

NASA Scientific and Technical Information Facility

FACILITY FORM 602

N71-12774 (ACCESSION NUMBER)	(THRU)
56 (PAGES)	G3 (CODE)
CR-111609 (NASA CR OR TMX OR AD NUMBER)	13 (CATEGORY)

DEC 1970
RECEIVED
NASA STI FACILITY
INPUT BRANCH

FFNo 672 Aug 65

13

UCSD-SP-70-04
September 1970

PLASMA CLOUDS IN THE MAGNETOSPHERE

S. E. DeForest and C. E. McIlwain

NGL-05-005-007

UNIVERSITY OF CALIFORNIA
SAN DIEGO

La Jolla, California

A
OCT 1970
RECEIVED
NASA STI FACILITY
INPUT BRANCH

Department of Physics

Space Physics Group

Cal. David Hamilton
#78

UCSD-SP-70-04
September 1970

PLASMA CLOUDS IN THE MAGNETOSPHERE

S. E. DeForest and C. E. McIlwain

NGL-05-005-007

UNIVERSITY OF CALIFORNIA
SAN DIEGO

La Jolla, California

OCT 1970
RECEIVED
NASA STI FACILITY
INPUT BRANCH

Department of Physics

Space Physics Group

UCSD-SP-70-04
September 1970

PLASMA CLOUDS IN THE MAGNETOSPHERE

by

S. E. DeForest and C. E. McIlwain
University of California, San Diego
La Jolla, California

Abstract

Equatorial observations by the geostationary satellite ATS-5 of the charged particles on auroral lines of force reveal the frequent injection of plasma clouds into the magnetosphere. These intrusions of hot plasma are found to have a one to one correspondence with magnetospheric substorms. The clouds are dispersed by the earth's magnetic and electric fields in a fashion which generates complicated energy structure.

Introduction

Previous equatorial observations of the magnetospheric plasma (Gringauz, 1961; Frank, 1967 a, b, and c; Vasyliunas, 1968; Frank, 1970; Frank and Owens, 1970) have been made from spacecraft which made rapid but infrequent traversals of the region between 5 and 20 earth radii or as in the case of the Vela spacecraft (Bame et al., 1967) remained at great distances.

These observations have shown the existence of a hot plasma which exhibits considerable structure in its radial dependence and in the energy spectra at each location. An excellent review of previous observations has been given by Gringauz (1969).

The ATS-5 data show a strong local time dependence and even more structure in the energy spectra than previously suspected. Data being presented here shows that this structure is a consequence of the injection of plasma in the vicinity of local midnight during magnetospheric substorms and of the energy dependent dispersion of the plasma in the earth's magnetic and electric fields. The injection and dispersion of the high energy tail of these plasma clouds have been previously reported by Konradi (1967), Arnoldy and Chan (1969), Pfitzer and Winckler (1969), and by Lezniak and Winckler (1970).

The present paper is also intended to serve as an introduction to the data being obtained from the University of California, San Diego (UCSD) plasma experiment on ATS-5 and to describe the general characteristics of the particle populations it has encountered.

Description of Experiment

The ATS-5 satellite was launched into synchronous orbit (6.6 R_e) in August 1969 and has been kept near 105 degrees west longitude since early September 1969. The orbital inclination is 2.30 degrees. Since the satellite continues to spin with a period of 0.79 seconds, the booms intended to provide gravity gradient orientation cannot be safely extended. The spinning motion improves the plasma data in that it provides the possibility of measuring important portions of the angular distribution. The spin axis is oriented parallel to the earth's rotational axis.

A number of particle and field experiments are carried by the ATS-5 satellite. The correlation of the results of these experiments is expected to be quite fruitful. However, the present paper is based almost entirely upon data from the UCSD plasma spectrometers. The only exception is the magnetometer data which has been kindly provided by T. Skillman of the Goddard Space Flight Center.

A complete description of the four spectrometers and associated electronics in the UCSD experiment will be published in the near future. Therefore only a short summary is given here.

The four cylindrical plate spectrometers consist of two pairs of electron and proton analyzers directed parallel and perpendicular to the spin axis. The parallel analyzers point north and thus detect particles coming from the northern hemisphere. The particles are detected with Bendix type 4010-3 channel electron multipliers which have narrow angle cones that give a 3 mm diameter sensitive area. Biases of -2700 volts are applied to the front of the multipliers for post-analysis acceleration of protons and + 500 volts for electrons. These biases result in a

constant high efficiency for the protons at all energies analyzed and for electrons below one kev. The efficiency of channel multipliers decreases at higher electron energies. This decrease has been accurately measured (Archuleta and DeForest) and all of the data presented here have been appropriately normalized to a constant effective efficiency. The potential of a grid immediately in front of the sensors is held at zero in the proton analyzers and at - 30 volts in the electron analyzers to suppress secondary electrons. All pulses greater than about 10^{-3} of the typical pulse size are counted so there is little change in efficiency with large changes in the channel multiplication factor. During the first year of continuous operation in orbit, no changes in efficiencies have been discernible.

Three simultaneous accumulations 0.26 seconds long are taken every 0.32 seconds. Two analyzer outputs are selected by ground command to feed two of the accumulators while the other two are alternately fed to the third accumulator. Accumulation is stopped for 4 microseconds after each pulse counted so that the small afterpulses which can occur during the first one or two microseconds after a particle is detected are not counted. Deadtime corrections are applied so that rates up to 10^6/sec are believed to be measured accurately.

The analyzers have an energy resolution of about 13% and a geometric factor such that dividing the counting rate by 4.3×10^{-5} cm^2 sr yields the differential energy flux in units of ev/cm^2 sec sr ev. The angular response to a uniform energy distribution extends over a rectangular solid angle of about 5 by 8 degrees.

The inner and outer plates of the analyzers are connected in parallel to two high voltage supplies which can be stepped through 62 exponentially spaced voltages 12% apart (with less than 0.1% accumulative error) thus varying the energy analyzed from 50 ev to 50,000 ev. Two zero voltage steps are also included to provide background measurements (in practice the background is usually low and is not subtracted).

The system can be commanded to cycle through all 64 steps each 20.48 seconds or in a number of other patterns. One frequently used mode alternates between a 20.48 second scan of all 64 steps and a 61.44 second period in which the analyzed energy is varied such that it tracks a peak in the counting rate spectrum of the detector which has been selected for the master channel. All of the data presented in this paper were taken in this track-scan mode with the parallel proton detector in the master channel, the perpendicular proton detector in the second channel (labeled "mate") and the electron detectors sharing the third subcommutated data channel.

Energy Spectra

The energy spectra observed by this experiment often contain a surprising amount of structure. An example is shown in Figure 1. The same data are plotted in Figure 2 but with a linear scale for the flux. The differential energy flux per unit energy is used for presentation of the data since it is proportional to the counting rate and, more importantly, it usually varies over a smaller range than the differential number flux or differential number density. The differential number flux can be quickly obtained from the differential energy flux by dividing by

the energy (in whatever units are desired since the energy per unit energy is dimensionless).

In Figure 1 a smooth curve is drawn through each data point which is marked by error bars which extend over the middle 68 percent of the probability distribution according to Poisson statistics. At high counting rates this corresponds to plus and minus one standard deviation.

Another surprising characteristic of the energy spectra is that structure often persists and only slowly changes over a period of many hours. Rather than making hundreds of individual plots to show the time development of the energy spectra, it is more efficient to employ the "sonagram" technique in which a function of two independent variables is encoded into a range of grey levels going from black to white. In this case, time is assigned to the horizontal axis, energy to the vertical axis and the differential energy flux to a range of grey levels with white representing the highest flux expected and black the lowest.

Figure 3 is a spectrogram of 24 hours of data from the parallel proton detector which includes the spectrum shown in Figure 1. Energy is plotted on a logarithmic scale with 50 ev at the bottom and 50 kev at the top. The time period starts at 2200 UT on January 5, 1970. Since the satellite is near 105 degrees west, subtraction of 7 hours from the universal time yields the local time (actually on this date it was nearing the end of a period of eastward drift and was at about 103 degrees west). The period thus begins and ends at 15 hours local time. Note that the peaks at 48, 28, 18, 10, and 3 kev in Figure 1 (traces G, E, D, C, and B) persisted for about 6, 8, 12, 18 and greater than 22 hours respectively. Note also that all of the peaks move fairly uniformly toward lower energies.

The peak labeled B in the upper part of Figure 3 which was at 3 kev in Figure 1 (1234 UT) began near 40 kev at 0000 UT on January 6, 1970 and reached 0.1 kev about 28 hours later. During this time, the angle between the detector and the magnetic field varied between about 10 and 30 degrees.

Interpretation of Energy Structure

Some progress has been made in the interpretations of these energy versus time patterns by starting with the assumption that the particles are following trajectories which conserve the first two adiabatic invariants and then searching for electric field patterns which predict the observed energy structure. A detailed presentation of these analyses is beyond the scope of this paper. The preliminary conclusions, however, provide a useful aid to the comprehension of the ATS-5 data. They are therefore stated here but without derivation:

1. Magnetospheric substorms correspond to a sudden intensification of the east-west electric fields in a narrow sector near midnight.
2. This electric field decreases with time but may persist for many hours.
3. A cloud of hot plasma is moved deep into the magnetosphere from regions of lower magnetic field which are presumably filled with plasma from the magnetosheath. Magnetic field lines inside the magnetopause are assumed to be closed.
4. The energetic particles in the cloud follow radically different paths due to the magnetic field gradient and curvature contributions to the drift velocity. In other words, energy, charge, and pitch angle dependent dispersion occurs.

5. The decrease in the east-west electric field with time leaves many of the particles on trapped orbits where they remain (unless removed by loss processes such as charge exchange or pitch angle scattering into the atmosphere) until the next substorm during which they are either moved back out or accelerated further in depending on their local time.
6. The radial component of the electric field is such that the local time average of the azimuthal drift velocity of zero energy particles is close to the corotation velocity.
7. The azimuthal drift velocity of zero energy particles is slower and greater than the corotation velocity before and after midnight, respectively.

Many of these conclusions are not new. The review by Axford (1969) describes most of the previous work which has lead to similar conclusions.

On the basis of the above statements, Figure 3 is interpreted as follows:

1. A plasma cloud (actually an overlapping pair of clouds) was injected during the substorms which had onsets at about 2245 and 2325 UT on January 5, 1970 (according to the Abisko and Leirvogur magnetometer records). No further injection events occurred until a pair of substorms at 1130 and 1300 UT on January 6, 1970 (according to the College magnetogram).
2. The 50 kev protons in the cloud gradient drifted west toward the ATS-5 which was approaching dusk local time and arrived at the satellite during a period of about 30 minutes beginning at about 2330 UT January 5. These protons form the beginning of the structure labeled "A" in the upper part of Figure 3.

5. The decrease in the east-west electric field with time leaves many of the particles on trapped orbits where they remain (unless removed by loss processes such as charge exchange or pitch angle scattering into the atmosphere) until the next substorm during which they are either moved back out or accelerated further in depending on their local time.
6. The radial component of the electric field is such that the local time average of the azimuthal drift velocity of zero energy particles is close to the corotation velocity.
7. The azimuthal drift velocity of zero energy particles is slower and greater than the corotation velocity before and after midnight, respectively.

Many of these conclusions are not new. The review by Axford (1969) describes most of the previous work which has lead to similar conclusions.

On the basis of the above statements, Figure 3 is interpreted as follows:

1. A plasma cloud (actually an overlapping pair of clouds) was injected during the substorms which had onsets at about 2245 and 2325 UT on January 5, 1970 (according to the Abisko and Leirvogur magnetometer records). No further injection events occurred until a pair of substorms at 1130 and 1300 UT on January 6, 1970 (according to the College magnetogram).
2. The 50 kev protons in the cloud gradient drifted west toward the ATS-5 which was approaching dusk local time and arrived at the satellite during a period of about 30 minutes beginning at about 2330 UT January 5. These protons form the beginning of the structure labeled "A" in the upper part of Figure 3.

3. Lower energy protons arrived at later times due to their smaller gradient and curvature drift velocity components.

4. The lowest energy protons on the dusk side of the cloud moved slowly with respect to the corotating satellite and, therefore, were encountered at about 0800 UT January 6.

5. The protons with energies of less than about 10 kev on the dawn side of the cloud initially moved farther from the satellite (the electric field part of the azimuthal drift velocity being greater than the magnetic field gradient and curvature components). As a consequence, the structure labeled "B" does not decrease to less than 3 kev until after ATS-5 reaches dawn (1300 hours UT).

6. The deep minimum in the spectrum between "B" and "C" (located at 5 kev in Figure 1) corresponds to the dividing line between protons which have drifted to the east and to the west. We believe that the intensities are low because these protons are coming back out from inner regions of the magnetosphere where the loss rates are high.

7. The trace of peaks labeled "C" corresponds to a second cloud of protons which was formed at the same time as the "A" and "B" sets of particles. Its origin is not understood, but the energy dispersion seems to be appropriate to an initial location on the day side of the magnetosphere. One possibility is that it is composed of that part of the previously trapped protons which was not ejected by the substorm electric fields.

8. Trace "D" is formed by protons from the same cloud as traces "A" and "B" but these protons have drifted westward all the way around the earth. Trace "F" is believed to be formed by the protons in this cloud which have made one additional circuit of the earth.

9. Trace "E" is formed by protons from the same cloud as trace "C", but these protons have also drifted around the earth.

10. Traces "G" and "H" are formed by protons which have dispersed about two-thirds of the way around the earth from clouds injected during the 1130 and 1300 UT substorms.

Injections During a Magnetic Storm

The time period of Figure 3 was relatively quiet: $K_p = 3$ for the first 5 hours and $K_p = 1$ for the remainder of the time. When there are greater magnetic disturbances, plasma is believed to be injected far inside the synchronous orbit and the ATS-5 satellite is presumably sampling the middle and outer regions of plasma activity.

Spectrograms of the data from the electron and proton spectrometer perpendicular to the spin axis during a relatively disturbed period are shown in Figure 4. The data from the parallel detectors for this period are shown in Figure 5. In these spectrograms the energy scales are proportional to $(E + 3 \text{ kev})^{-1}$. The electron scale is inverted so that zero energy for both protons and electrons is located at the time marks between the two spectrograms. Infinite energy on these scales is located at the bottom time marks for protons and at the time marks above the electron spectra for electrons. These peculiar energy scales have the property of straightening out many of the energy dispersion traces and permits easy determination of injection times by extrapolation back

to the time infinite energy particles would have arrived. The components of the magnetic field perpendicular and parallel to the spin vector are plotted along with the spectrograms of the perpendicular analyzers. The magnitude of the field and the angle to the spin vector are plotted along with the spectrograms of the parallel analyzers. These magnetic field data are not corrected for the changing spacecraft fields. For the measurements of the perpendicular component of the magnetic field, only the coarse (33 γ step size) data was used causing an additional uncertainty of about $\pm$ 10 γ. A guide to the reading of these spectrograms is given in Appendix A.

Figures 4 and 5 cover the time period from 1500 UT on January 1, 1970 to 2100 UT on January 2, 1970. The K_p values during this period were 3, 3-, 2, 3-, 4+, 5+, 4, 4, 4+, and 4. Low latitude magnetograms exhibited 50 γ decreases due to asymmetrical ring currents (see Solar-Geophysical Data No. 311, Part 2, page 60).

Figure 6 shows traces of some of the spectral peaks exhibited in Figure 4 with labels for future reference.

Figure 7 is a set of five magnetograms for this time period which have been replotted on a common scale (courtesy Dr. Syun Akasofu). The "M"s mark the time of local midnight at each observatory and the vertical lines labeled alphabetically indicate the onset times of the major substorms at about 1620 and 2220 UT on January 1, 1970 and 0310, 0350, 0720, 1125, 1600, and 1830 UT on January 2, 1970.

The proton and electron curves labeled "A" in Figure 6 are believed to be due to the dispersion of a plasma cloud injected during the 1620 UT substorm on January 1, 1970 (also labeled "A" in Figure 7). Assuming that

the cloud was formed in the vicinity of local midnight, both species have traveled about half-way around the earth with the electrons taking an eastward path and the protons a westward path. The low energy protons and electrons in the dusk side of this cloud were apparently encountered at about 0100 UT which corresponds to dusk local time. Since the initial location of the dusk side of clouds rarely extends to local times earlier than 2100 UT, these low energy particles were presumably convected 3 or 4 hours in local time to the west during the first 8 hours after injection.

It is believed each of the labeled curves in Figure 6 is produced by a cloud injected during the substorm designated by the same letter in Figure 7.

The dispersion curves for the "B" substorm are similar to those of the "A" substorm except that the satellite was closer to the dusk side of the cloud so that the low energy particles were encountered only 4 hours after injection began.

Event "C" at 0310 UT was preceded by a precursor at 0249 UT and was followed by the stronger event "D" at 0350 UT (before the arrival of low energy particles from the "C" event).

The western edge of the cloud injected during the "D" event was initially quite close to the satellite so that low energy particles arrived within minutes after the onset. The satellite was soon within the main body of plasma being convected in from regions of smaller magnetic field.

The ATS-5 was near local midnight at the time of event "E" so that particles of all energies arrived with little delay.

By the time of the "F" event, the satellite was approaching dawn so that the energetic electrons with their eastward directed gradient drift velocity component arrived first but were quickly followed by low energy particles (being rapidly convected to the east) and eventually by protons with energies up to 20 kev which were also moving eastward but at a lower rate due to their opposing gradient drift velocity component. As in event "A", the protons on the dusk side of the cloud drifted westward and were detected along the second "F" trace in the lower half of Figure 6.

Energy Spectra During the Storm

In addition to the structure produced by energy dispersion, a number of other types of peculiarities in the energy spectra are observed during magnetic storms. To exhibit some of these features better, the middle part of the time period in Figures 4 and 5 is replotted in Figures 8 and 9 with the time scale expanded by a factor of two and with logarithmic energy scales.

Nine sets of spectra are plotted in Figures 10 through 18 to permit a more detailed study of the spectral features. The electron spectra are plotted on the left half and the proton spectra on the right half of these figures. The spectra of the electron spectrometer directed parallel to the spin is shifted down by a factor of 100 and the perpendicular proton data is shifted up by a factor of 100 so that both upper curves correspond to the perpendicular detectors. The error bars again correspond to the middle 68 percent of the Poisson distribution. Points at which zero counts were obtained are indicated by upward pointing triangles.

Figures 15 and 16 contain points at which no data was available so that earlier data was used. This substitution of earlier data is indicated by downward pointing triangles. The lines below the "BKGD"s represent the measured background for each of the four detectors. Note that care must be exercised in referring to the background levels since the background for the upper curves frequently falls in the vicinity of the lower curves. A more complete description of these plots is given in Appendix B.

Before proceeding, note that spurious energy structure can be generated in at least two ways. One is that any spin modulation can "beat" with the energy sampling. The long-time averages used in the present plots tend to minimize this effect. The other one is that the detectors sharing the subcommutated data channel have only every other energy step sampled during each scan. The peak tracking system is such that on subsequent scans the other half of the steps may be sampled, but, in the meantime, the spectrum may have changed. During the period now being considered the electron detectors were sharing the subcommutated channel so their spectra frequently show a "ripple" due to spectral changes between the times of the interlaced scans. This effect is also the cause of horizontal bars in the electron portion of the spectrograms during rapid time changes.

Figure 10 shows the spectra obtained at the beginning of the time period covered by Figure 4. The structure can be shown to be caused by the dispersion of clouds injected at earlier times.

Figure 11 taken 2 hours later at 1715 UT on January 1, 1970 shows how all of the fluxes below 1 kev were reduced following the "A" event at 1620 UT. These fluxes had, in fact, already made changes by 1600 UT indicating the possibility that the electric fields in the dayside magnetosphere

may be modified well in advance of the sudden substorm enhancements in the vicinity of midnight.

Figure 12 shows spectra in which the electrons measured parallel to the spin vector are almost 100 times greater than perpendicular fluxes in the energy region around 300 ev. Simultaneously, the low energy perpendicular proton fluxes are about twice as high as the parallel proton fluxes. Comparison of Figures 4 and 5 reveals that this phenomenon persisted for a period of over 4 hours. Perhaps the extra parallel electrons were brought into this region of space to compensate for the excess positive charge arriving in the form of energetic protons from the cloud injected by event "A".

Figure 13 shows the spectra after the arrival of the low energy electrons from the "B" event. Note the sharpness of the dividing line at 1 kev between these electrons and those between 1.2 and 6 kev which were probably injected during much earlier events and therefore had more time to decay.

Figure 14 shows the spectra after the arrival of the energetic electrons from event "D". Between 5 and 50 kev, the electron spectra are very similar to a Maxwellian distribution with a temperature of 6 kev. The low energy portion of the parallel electron spectrum will be discussed below.

Figure 15 shows the spectra just before event "E" while the magnetic field was near its minimum value of about 60 γ. Both dashed lines correspond to an isotropic Maxwellian distribution with a temperature of 2.46 kev and a density of 5.5 electrons/cm^3. The measured spectra match this fit to within ± 30% over the range from 0.8 to 24 kev, but they are

about a factor of 5 higher at 80 ev and remain constant above 30 kev instead of rapidly decreasing.

Figure 16 shows the spectra just after event "E" while the magnetic field was near 150 γ. First, note the depletion of the parallel electrons which begins sharply at 1000 ev. A similar sharp decrease at 150 ev can be seen in Figure 14. Step-like spectral features such as these are referred to as "precipices". Figures 5 and 9 show that this phenomenon persisted for about 1-1/2 hours after event "D" and for about 9-1/2 hours after event "E". The fluxes below the precipice energy are not reduced to background, and they often contain nearly monenergetic peaks which move in unison with changes in the precipice energy. Examination of the perpendicular proton and electron data for this and other periods has yet to reveal any peculiarities directly associated with the occurrence of parallel electron precipices. The parallel proton data, however, invariably exhibits extreme modulation at the spin frequency at all energies less than about twice the electron precipice energy. Since it is believed that the detector look direction is aligned within 3 degrees of the spin axis, these modulations, which can be as great as 50 to 1, cannot be due to structure in the pitch angle distribution unless the proton trajectories are perturbed in the near vicinity of the spacecraft. It is not yet known whether these effects in the parallel detectors could be caused by surface charges on the cylinder of solar cells which extend beyond the aperture of these detectors. In any case, it seems possible that these effects are at least indirectly caused by an interesting feature of the ambient plasma such as field aligned currents. It can be seen in Figure 16 that there is, in fact, a large flux of

about a factor of 5 higher at 80 ev and remain constant above 30 kev instead of rapidly decreasing.

Figure 16 shows the spectra just after event "E" while the magnetic field was near 150 γ. First, note the depletion of the parallel electrons which begins sharply at 1000 ev. A similar sharp decrease at 150 ev can be seen in Figure 14. Step-like spectral features such as these are referred to as "precipices". Figures 5 and 9 show that this phenomenon persisted for about 1-1/2 hours after event "D" and for about 9-1/2 hours after event "E". The fluxes below the precipice energy are not reduced to background, and they often contain nearly monenergetic peaks which move in unison with changes in the precipice energy. Examination of the perpendicular proton and electron data for this and other periods has yet to reveal any peculiarities directly associated with the occurrence of parallel electron precipices. The parallel proton data, however, invariably exhibits extreme modulation at the spin frequency at all energies less than about twice the electron precipice energy. Since it is believed that the detector look direction is aligned within 3 degrees of the spin axis, these modulations, which can be as great as 50 to 1, cannot be due to structure in the pitch angle distribution unless the proton trajectories are perturbed in the near vicinity of the spacecraft. It is not yet known whether these effects in the parallel detectors could be caused by surface charges on the cylinder of solar cells which extend beyond the aperture of these detectors. In any case, it seems possible that these effects are at least indirectly caused by an interesting feature of the ambient plasma such as field aligned currents. It can be seen in Figure 16 that there is, in fact, a large flux of

protons in the region of 1.5 to 3.0 kev which has no counterpart in the perpendicular spectrum. Figure 9 shows, however, that this feature was intense for less than one hour.

Still another interesting energy structure in Figure 16 is the sharp peak in both proton spectra at 70 ev. Peaks of this character would be produced if the satellite were forced to attain a potential of -70 volts with respect to the plasma in order to maintain a zero flux of charge. If this interpretation is correct, it indicates that very few cold ions of ionospheric origin were present.

Figure 17 shows the spectra 2 hours after the "F" event when the satellite was near dawn local time. The parallel electron spectrum exhibits a precipice at about 500 ev accompanied by a nearly mono-energetic peak at 350 ev. It is believed that the protons with energies greater than 10 kev have traveled around the dayside of the earth and that the lower energy protons and all of the electrons have been convected directly from the region near midnight local time.

Figure 18 shows the spectra about 4-1/2 hours after the "F" event. The parallel electron precipice has moved down to 150 ev and the dividing line between eastward and westward drifting protons has moved to about 5 kev.

Integrals Over the Spectra

Four different integrals for each of the four spectra in Figures 10 through 18 are given at the top of each plot. The units and other details of these integrals are described in Appendix B.

In Figure 19, running 5.5-minute averages of 10 of the integrals are plotted for the entire time period covered by Figures 4 and 5. The

integrals are computed only for the measured part of the distributions with no extrapolations to higher or lower energies. The densities per unit solid angle have been multiplied by 4π to permit quick estimates of the total number densities.

The electron energy fluxes observed during the storm were quite adequate to produce bright auroral light emissions. The perpendicular and parallel electron energy fluxes were typically above 10 and 6 ergs/cm^2 sec sr and had maxima at about 30 and 14 ergs/cm^2 sec sr, respectively.

The integrals can be seen to have large long-term variations but to have few short-term variations larger than a factor of three. The auroral emissions during the storm presumably exhibited the usual sharp spacial features such as arcs and rays and also strong short-term variations. If these auroral features have no direct counterpart in the equatorial plasma, they must be due to differences in precipitation rates and other phenomena such as field aligned currents. Unfortunately, as yet it is not accurately known what parts of the auroral regions are on the magnetic field lines encountered by the ATS-5 satellite.

The particle pressure is usually dominantly due to protons, but the electrons often make an important contribution. Occasionally the electron pressure is over twice the proton pressure as it was, for example, at 1200 UT January 2, 1970.

The perpendicular particle pressure and the magnetic field pressure exhibit no simple dependence upon each other, and both positive and negative correlations are observed. This may indicate the presence of strong external forces. The presence of external forces may also be

indicated by the relative stability of the plasma even though the particle pressure exceeded the magnetic field pressure for many hours during the storm. In particular, during the 20 minutes preceding event "E" (at 0725 UT) the particle pressure was over 3 times that of the magnetic field.

The detailed energy structure encountered by the ATS-5 satellite varies radically from day to day since it depends upon the time and intensity of all of the substorms during at least the preceding 24 hours. The integrals of the spectra at any particular local time are much more consistent, however. To illustrate this, the integrals from the perpendicular detectors have been examined during 29 days in January 1970 to obtain minimum, maximum, and "typical" values at six different local times. The results, along with values for the ratio of pressures, are given in Table 2.

The number densities of electrons and protons are rarely equal, although they often differ by less than 15%. In the local time region within about ± [illegible] hours of dusk, the satellite is probably often within the plasmasphere so that the cold plasma of ionospheric origin (which is not being measured) dominates the number densities. At other local times it is believed that the missing charge is frequently to be found in hot plasma components outside the energy range of 50 ev to 50 kev. In particular, it is believed that protons in the 10 to 50 ev and 50 to 100 kev often make important contributions to the total density.

Summary

Analysis of the data obtained by the UCSD experiment on the ATS-5 satellite has yielded the following conclusions:

1. A hot cloud of plasma is injected into the midnight sector of the magnetosphere during each substorm.
2. Energy and pitch angle dependent dispersion produces:
   a. sharp and long lived energy structure, and
   b. large energy dependent pitch angle anisotropies.
3. The main body of plasma may not directly reflect the strong space and time variations usually exhibited by auroral precipitation patterns.
4. Increases in the electric field associated with a substorm can further accelerate parts of the plasma previously injected. It therefore seems probable that these increases not only provide an input, but also cause at least the initial steps in the "radial diffusion" responsible for the radiation belts.

Acknowledgements

The authors wish to express their appreciation to all of the many people who contributed to the success of this experiment. We are particularly grateful for the special efforts made by Dr. John Naugle of NASA Headquarters, Dr. R. Walker Fillius and Mr. Eugene Strein of UCSD, by the Analog Technology Corporation and by the Goddard Space Flight Center. We would like to thank Dr. Robert La Quey and Dr. Ian Axford for their helpful comments and advice.

This research is supported in part by NASA Contract NAS 5-10364 and NASA Grant NGL 05-005-007.

APPENDIX A

DESCRIPTION OF ATS-5 SPECTROGRAMS

Format

The spectrograms are produced in pairs: one showing the spectra from the perpendicular proton and the perpendicular electron analyzers and one showing the spectra from the parallel proton and electron analyzers. They are labeled by a large $\perp$ or $||$ on the middle left side. The proton part is always below the electron part. The day of the year (January 1 equals day 1) and year is given at the bottom. The month, day in month, and year are also given at the left just above the $\perp$ or $||$ label. The times at the beginnings and ends of the spectrograms can be arbitrarily set, and can cover any desired time span. Time scales covering as little as 10 minutes and as great as 4 days have been used. When more than one day is encompassed, either negative hours or hours greater than 24 are used to prevent any ambiguity. Grey scales are located at the right. Six different integrals are plotted in grey coded bands in the upper part along with magnetic field quantities. At the very top are two data quality indicators.

Grey Scale Interpretation

The primary value of spectrograms is their ability to reveal patterns in the energy-time plane. The determination of actual flux levels from them is of secondary importance. For this reason, and because of the loss in time resolution, the option which produces a coded pattern with which accurate flux values can be obtained is now rarely used. Color coding also permits accurate values to be obtained, but is more

expensive than grey coding. In the present case, color is reserved for adding another dimension: by superimposing the perpendicular and parallel spectrograms with color filters limiting each to one-half of the visible spectrum, the energy and time dependence of the pitch angle anisotropies are clearly displayed as patterns of different shades of color.

Should one desire to estimate the flux at a given point on a spectrogram, first locate the corresponding level on the grey scale at the lower right and determine the value of "G" on the scale marked 0 to 3. The differential energy flux in ev/cm^2 sec sr ev is then given by

$$(10^G - 1)\, 10^{b + 4.367}$$

where b is given by "EL" in the lower left corner of the spectrogram for the electron fluxes or "PR" for the proton fluxes. The value of "ST" in the lower left corner gives the change in G between each of the 33 discrete grey levels available.

One option available is to let the grey scale recycle repeatedly instead of simply saturating. This option with a small value of "ST" is used to reveal small variations over a wide dynamic range of fluxes.

Energy Scales

The computer program which generates the spectrograms can utilize any arbitrary function of energy for the energy scales for exhibiting all or any part of the measured spectra. The entire range from 50 ev to 50 kev is usually plotted with one of the two types of scales:

1. logarithmic with 50 ev at the bottom for both protons and electrons.

2. proportional to $1/(E + 3 \text{ kev})$ with the electron part inverted and sharing the same point with the protons at zero energy. The bias of 3 kev was arbitrarily chosen to give a good presentation of the 50 ev to 50 kev energy range. If the scale, S, is taken to be 0.0 at infinite proton energy, 1.0 at zero electron and proton energy and 2.0 at infinite electron energy, then

$$S = \frac{E(1-q) + 3 \text{ kev}}{E + 3 \text{ kev}}$$ where E is the particle energy in kev

$q = \pm 1$ depending on the sign of the particle's charge. Note that at low energies, $S \simeq 1 + qE/3$ kev. Time tic marks are located at S = 0, 1, and 2. The extrapolation of dispersion curves back to the time marks (at S = 0 or 2) yields the time infinite energy particles would have arrived, and therefore, the time of the event responsible for the dispersing particles. The slopes of the high energy parts of dispersion curves give a measure of the distance of the satellite from the regions in which the particles were perturbed, but it is apparently necessary to include electric field effects to obtain useful accuracy.

Subsidiary Data

A number of useful quantities are given in the lower left hand corner.

The analyzers in the "master" and "mate" channels are identified by numbers following "MASTR" and "MATE" according to the scheme:

1. perpendicular electron analyzer
2. perpendicular proton analyzer
3. parallel electron analyzer
4. parallel proton analyzer

TA = averaging time for the spectra in minutes.

TS = time between spectral averages in minutes.

TM = averaging time for the magnetic data in minutes.

The seven bit command word is given immediately below "COMMAND". The first three bits give the channel assignments and are therefore redundant to the master and mate identifications given above. Bits 4 and 5 specify the operating mode according to the scheme:

bit	4	5	Mode
	0	0	track-scan
	0	1	single step scan only
	1	0	track only
	1	1	double step scan only

Bits 6 and 7 not set to zero correspond to other modes which are rarely used.

"ST", "EL", and "PR" are described above.

"PSNG" specifies the quantity being plotted in the spectrogram according to the scheme:

1. differential energy flux
2. differential number flux
3. ratios of the flux averaged over "TS" minutes to the flux averaged over the previous "TA" - "TS" minutes.
4. ratios of adjacent energy steps.

Options other than the first are used only in special studies. If the option to make the background black rather than white has been used, then "PSNG" will be negative. A black background is preferred for slides that are to be projected.

Magnetic Field

Data from the ATS-5 magnetometer have been kindly supplied by T. Skillman of the Goddard Space Flight Center and are plotted above the spectral data along with lines at 0, 50, 100 and 150 gammas. The data are not corrected for the effects of time changes in the spacecraft current systems. These perturbations can be as large as 15 gammas. The absolute value of the magnetic field component parallel and perpendicular to the spin axis is given by the darker and lighter points respectively (and usually the upper and lower respectively) with the spectrograms of the perpendicular analyzers. The perpendicular component is obtained using only the coarse (33 gamma step size) data and is thus uncertain by at least ± 10 gammas. Most of the scatter in this component is due to using only the coarse data.

The magnitude of the field and the angle of the field to the spin axis are given by the lighter and darker points respectively (and usually the upper and lower respectively) with the spectrograms of the parallel

analyzers. The angle to the spin axis is given in degrees. Both the magnitude and angle are subject to the additional uncertainties in the perpendicular component.

Integrals

Above and below the magnetometer data are six strips in which various quantities are logarithmically encoded in a grey scale such that a ratio of about 2000 to 1 is covered in going from black to white.

In the 1st, 2nd, 3rd, and 5th strips, the following integrals from the perpendicular and parallel analyzers are plotted with perpendicular and parallel spectra respectively:

Label	Quantity	Value at Midpoint of Grey Scale
PR N DEN	proton number density	1.0 proton/cm^3
EL N DEN	electron number density	1.0 electron/cm^3
E E FLX	electron energy flux	1.0 erg/cm^2 sec sr
PR E FLX	proton energy flux	1.0 erg/cm^2 sec sr

In the 4th strip labeled "PRESSURE", the total perpendicular electron plus proton pressure is plotted with the spectrogram of the perpendicular detectors with a midpoint value of 10^{-8} dynes/cm^2. In the 4th strip with the parallel data, the magnetic field pressure is plotted with a midpoint value of 2×10^{-8} dynes/cm^2.

In the 6th strip (near the top) labeled "PAR NFLX" the parallel electron number flux is plotted with the spectrogram of the perpendicular detectors with a midpoint value of 10^8 electron/cm^2 sec sr. In the top strip with the parallel data, the parallel proton number flux is plotted with a midpoint value of 10^7 protons/cm^2 sec sr.

Data Quality Indicators

At the very top of the spectrogram is a line which increases in breadth with an increasing percentage of missing data. In the track-scan mode, about 73 percent of the potential data is usually "missing" since 75 percent of the time is spent tracking a peak in a narrow spectral region. When data are not available, previous data are used unless the time gap is greater than 30 minutes in which case the spectrograms are left blank. The top line, of course, goes to its maximum width during gaps in the data. The magnetometer data is not plotted during such gaps. Care must be exercised to avoid false interpretations of spectrograms containing data padded in from an earlier time.

Just below the missing data line is a line which becomes darker and thicker with increasing numbers of bad points. Often the quality of data transmission is such that over one percent of the data points are bad. Even the highest quality data being obtained are usually incorrect more than 0.1 percent of the time. This corresponds to over 800 bad data points per day of data. A data editing scheme has been devised which eliminates approximately 99 percent of the bad data and rarely removes data later judged to be good. Failure to remove bad points usually occurs when the false data happen to form a self-consistent context. This type of failure to edit properly is responsible for the two white areas in the lower right of Figure 4. The bad data indicating line reaches its maximum thickness when there are more than 10 bad points in the four spectra measured during the time covered between averages (equal to "TS").

APPENDIX B

DESCRIPTION OF ATS-5 SPECTRAL AVERAGE PLOTS

Format

The spectra from the two electron and the two proton analyzers are plotted in adjoining log-log plots with borders at 30 ev and 100 kev. The range of the vertical scale is variable and depends upon whether the differential energy flux or the differential number flux is being plotted. The parallel electron spectrum is shifted down by a factor of 100 (i.e. x 0.01) and the perpendicular proton spectrum is shifted up by a factor of 100 (i.e. x 100). These shifts usually provide adequate separation and place the perpendicular spectra above the parallel spectra in each case.

The universal time at the midpoint of the data being averaged over is given twice at the top of the plots. On the left hand (electron) side, the time is given in hours, minutes, tenths of minute, month, day of month, and year, and is followed by the averaging time in minutes. On the right hand (proton) side, the time is given in hours (to the nearest one thousandth of an hour), day of year (January 1 equals day 1), and the year. The local time in hours and minutes is sometimes added on the left side.

Also given near the top are four different integrals over each of the four spectra. The integrals for the perpendicular data are given above the integrals for the parallel data. Following two of these sets of integrals will be found the words "MASTER" and "MATE" to indicate which analyzers are occupying the two non-subcommutated data channels.

When in the track mode, the "master" analyzer controls the peak tracking system. The operating mode (for example the scan only or track-scan modes) of the system is given on the right side.

Error Bars

Vertical bars which encompass the middle 68.26 percent of the Poisson distribution are given at each data point. At high rates, they correspond to plus and minus one standard deviation. The approximation $N_{\pm} = N \pm \sqrt{N}\ (1.0 - 0.17/N)$ is used where N is the total number of counts accumulated at the point.

When in the track-scan mode, there are about four times the number of accumulations at the points near the energy of the peak being tracked than at other energies. Also the spectra from the "Master and "Mate" channels will have about twice the accumulation time as the other two (subcommutated) spectra.

When in the single step scan only mode, every other data point in the subcommutated spectra will be missing. This under-sampling of the spectra can lead to substantial errors in the smooth line drawn through the data points since structure as sharp as the instruments' resolution is frequently observed.

If zero counts are obtained, then the error bar is replaced by a triangle pointing up to the line which is placed at one-half the flux corresponding to one count being accumulated.

If no data are available for a point during the time period being averaged over, then the flux obtained during a preceding time period is inserted. In this case, the error bar is replaced by a triangle pointing down to the data point.

Integrals Over the Spectra

The four integrals given for each analyzer at the top of the plots are of course intrinsically directional quantities. The parallel cases correspond to pitch angles near α = the angle of the spin vector to the magnetic field vector, and the perpendicular cases correspond to averages over the pitch angle range of 90 $\pm \alpha$ degrees. The integrals are taken only over the measured range of 50 ev to 50 kev and are, therefore, lower limits.

The number densities in particles/cm^3 are labeled "DEN" and correspond to 4 π times the directional number densities in particles/cm^3 sr.

The particle pressures in 10^{-9} dynes/cm^2 are labeled "PRES". They correspond to 8 $\pi/3$ times the directional energy densities in ergs/cm^3 sr. The multiplication by 8 $\pi/3$ simplifies computation of the total particle pressure perpendicular to the magnetic field vector.

The directional energy fluxes in ergs/cm^2 sec sr are labeled "E FLX".

The directional number fluxes in 10^6 particles/cm^2 sec sr are labeled "N FLX".

REFERENCES

Archuleta, R. and S. E. DeForest, Efficiency of channel electron multipliers for electrons of 1-50 kev, accepted for publication in Rev. Sci. Inst.

Arnoldy, R. L., and K. W. Chan, Particle substorms observed at the geostationary orbit, J. Geophys. Res., 74, 5019, 1969.

Axford, W. I., Magnetospheric convection, Rev. of Geophys., 7, 421, 1969.

Bame, S. J., J. R. Asbridge, H. E. Felthauser, E. W. Hones, and I. B. Strong, Characteristics of the plasma sheet in the earth's magnetotail, J. Geophys. Res., 72, 113, 1967.

Frank, L. A., On the extraterrestrial ring current during geomagnetic storms, J. Geophys. Res., 72, 3753, 1967a.

Frank, L. A., Initial observations of low-energy electrons in the earth's magnetosphere with OGO 3, J. Geophys. Res., 72, 185, 1967b.

Frank, L. A., Several observations of low-energy protons and electrons in the earth's magnetosphere with OGO 3, J. Geophys. Res., 72, 1905, 1967c.

Frank, L. A., and H. D. Owens, Omnidirectional intensity contours of low-energy protons ($0.5 \leq E \leq 50$ kev) in the Earth's outer radiation zone of the magnetic equator, J. Geophys. Res., 75, 1269, 1970.

Gringauz, K. I., The structure of the ionized gaseous envelope of the earth according to the data of direct measurements of local charged-particle concentrations carried out in the USSR, Space Res., 2, 574, 1961b.

Gringauz, K. I., Low-energy plasma in the Earth's magnetosphere, Rev. of Geophys. 7, 339, 1969.

Konradi, A., Proton events in the magnetosphere associated with magnetic bays, J. Geophys. Res., 72, 3829, 1967.

Lezniak, T. W., and J. R. Winckler, An experimental study of magnetospheric motions and the acceleration of energetic electrons during substorms, University of Minnesota Cosmic Ray Tech. Rept. CR-149, April 1970.

Pfitzer, K. A., and J. R. Winckler, Intensity correlations and substorm electron drift effects in the outer radiation belt measured with the OGO 3 and ATS 1 satellite, J. Geophys. Res., 74, 5005, 1969.

Solar Geophysical Data, No. 311, Part 2, page 60, 1969.

Vasyliunas, V. M., A survey of low-energy electrons in the evening sector of the magnetosphere with OGO 1 and OGO 3, J. Geophys. Res. 73, 2839, 1968a.

FIGURE CAPTIONS

1. Differential energy flux of protons near the loss cone at L = 6.8 earth radii averaged over a 10.9 minute period centered on 1233.8 UT Jan. 6, 1970. The dashed line corresponds to a differential number flux of 100 protons/cm^2 sec sr ev.

2. Same as Figure 1 except with a linear flux scale.

3. A spectrogram of the proton differential energy flux during Jan. 6, 1970. The upper half identifies some of the dispersion curves.

4. Spectrogram of the perpendicular proton and electron fluxes (4.1 minute averages taken every 1.37 minutes) from 1500 UT Jan. 1, 1970 to 2100 UT Jan. 2, 1970. The energy scales are proportional to $(E + 3 \text{ kev})^{-1}$. A description of this and the following spectrograms is given in Appendix A.

5. Same as Figure 4 but of the fluxes parallel to the spin axis which is aligned with the earth's rotational axis.

6. Dispersion curves found in Figure 4 which are believed to be associated with the substorms identified by the same letters in Figure 7.

7. Five magnetograms covering the same time period as Figures 4, 5, and 6. The "M"s mark local midnight at each station and the vertical lines mark the onset of 8 substorms.

FIGURE CAPTIONS

1. Differential energy flux of protons near the loss cone at L = 6.8 earth radii averaged over a 10.9 minute period centered on 1233.8 UT Jan. 6, 1970. The dashed line corresponds to a differential number flux of 100 protons/cm^2 sec sr ev.

2. Same as Figure 1 except with a linear flux scale.

3. A spectrogram of the proton differential energy flux during Jan. 6, 1970. The upper half identifies some of the dispersion curves.

4. Spectrogram of the perpendicular proton and electron fluxes (4.1 minute averages taken every 1.37 minutes) from 1500 UT Jan. 1, 1970 to 2100 UT Jan. 2, 1970. The energy scales are proportional to $(E + 3 \text{ kev})^{-1}$. A description of this and the following spectrograms is given in Appendix A.

5. Same as Figure 4 but of the fluxes parallel to the spin axis which is aligned with the earth's rotational axis.

6. Dispersion curves found in Figure 4 which are believed to be associated with the substorms identified by the same letters in Figure 7.

7. Five magnetograms covering the same time period as Figures 4, 5, and 6. The "M"s mark local midnight at each station and the vertical lines mark the onset of 8 substorms.

8. Spectrogram of the perpendicular fluxes (2.74 minutes averages taken every 1.37 minutes) of the middle part of the time period covered in Figure 4. Simple logarithmic energy scales are used.

9. Same as Figure 8 but of the parallel fluxes.

10. The four spectra averaged over 4.1 minutes showing the energy structure found near the beginning of the time period covered by Figures 4 and 5. Note that the system is in the track-scan mode which performs only 3 scans in a 4.1 minute period. This means that except in the vicinity of the energy of the peak being tracked, each energy step is sampled for only three 0.26 second intervals during the 4.1 minutes. Furthermore, the electron data are subcommutated so that there are only three 0.26 second samples taken for each pair of adjacent energy steps. Care must be exercised to associate the correct background level with the proper spectrum.

11. The spectra after the depletion at low energies associated with event "A".

12. Spectra showing high energy protons from event "A" and enhanced low energy parallel electron fluxes.

13. Spectra after the encounter with low energy electrons from event "B".

14. Spectra after the arrival of electrons from event "D". The "ripple" in the electron spectra is due to time changes between the interlacing scans.

15. Spectra just prior to event "E".

16. Spectra showing a "precipice" in the parallel electrons, a 3 kev peak in the parallel protons, and sharp peaks in both the parallel and perpendicular protons at 70 ev.

17. Spectra showing a 350 ev peak in the parallel electrons.

18. Spectra showing the parallel electron fluxes to be about a factor of three less than the perpendicular fluxes and the 100 to 1000 ev parallel proton fluxes about a factor of 3 greater than the perpendicular proton fluxes.

19. 5.46 minute averages computed each 2.73 minutes of four different types of integrals over the 50 ev to 50 kev spectra.

Table 1

50 ev to 50,000 ev Spectral Integrals

	ELECTRONS						PROTONS					
LOCAL TIME	0	3	6	12	18	21	0	3	6	12	18	21
					NUMBER DENSITY IN PARTICLES/CM^3							
Minimum	.07	.22	.17	.06	.02	.04	.7	.6	.7	.3	.5	.6
Maximum	8.3	4.8	2.9	1.2	1.9	4.4	3.8	3.5	1.9	2.2	2.2	2.4
Typical	2.0	2.0	1.2	.4	.10	.4	1.2	1.2	1.2	.9	.8	1.1
					ENERGY FLUX IN ERGS/CM^2 SEC SR							
Minimum	.21	.38	.42	.26	.04	.10	.16	.13	.05	.13	.14	.14
Maximum	9.4	15.2	14.6	2.3	1.01	7.2	.61	.47	.47	.76	.63	.85
Typical	3.0	3.0	1.5	1.0	.40	.5	.3	.3	.3	.22	.30	.30
					NUMBER FLUX IN 10^6 PARTICLES/CM^2 SEC SR							
Minimum	15	37	32	15	2	9	6	4	4	2	4	5
Maximum	1510	1020	832	122	162	864	25	17	16	15	23	25
Typical	300	300	200	70	30	60	12	10	8	7	8	10
					PRESSURE IN 10^{-10} DYNES/CM^2							
Minimum	2.7	6	6	4	0.4	1	66	51	25	31	54	56
Maximum	190	266	173	25	14	128	235	196	169	242	255	327
Typical	50	60	30	12	7	8	140	120	90	80	90	120
					RATIO OF TOTAL PARTICLE PRESSURE TO THE MAGNETIC FIELD PRESSURE							
Minimum	.13	.13	.08	.04	.09	.09						
Maximum	2.7	1.07	.52	.21	.62	1.06						
Typical	.4	.4	.2	.12	.2	.25						

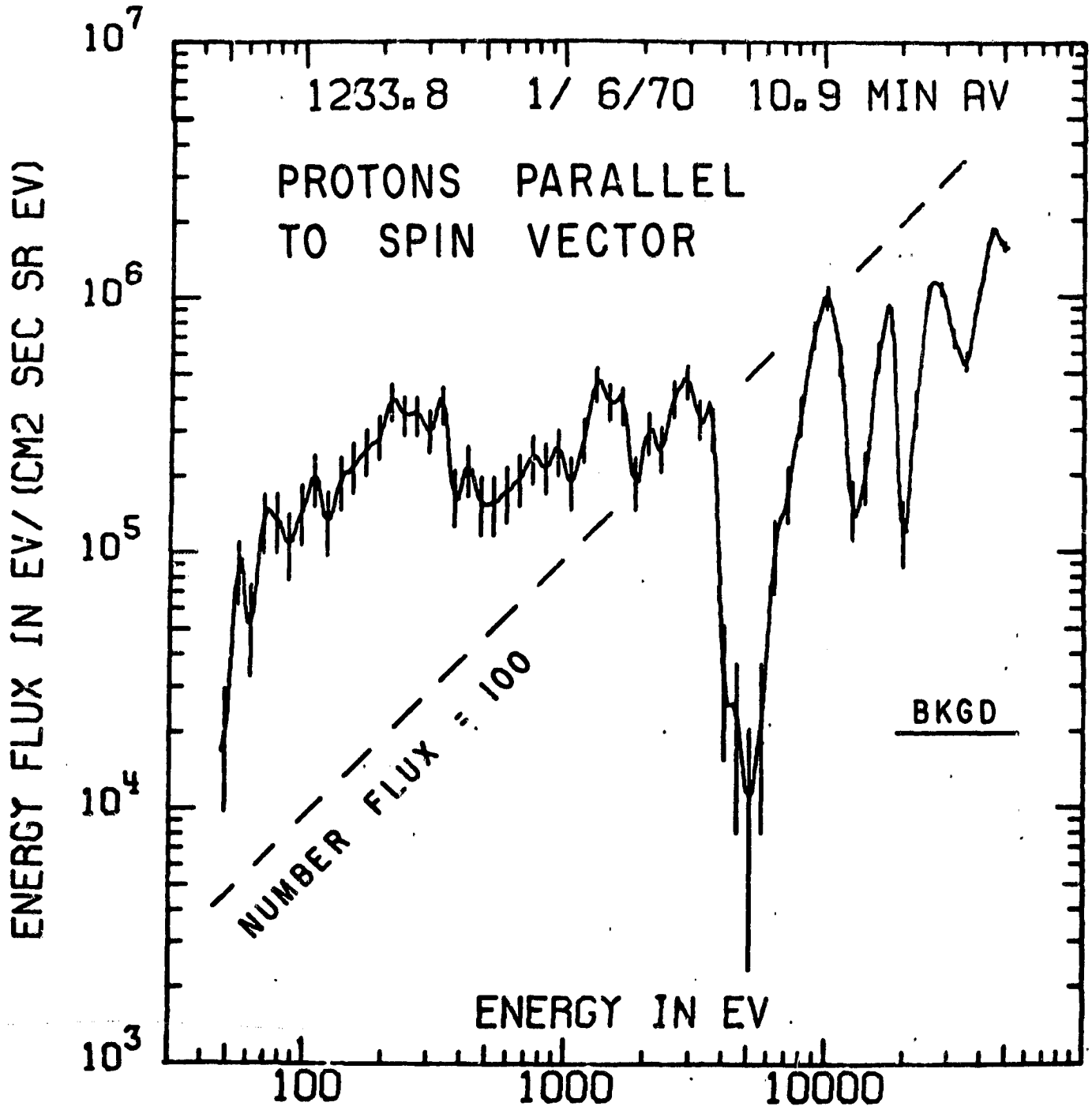
1233.8 1/ 6/70 10.9 MIN AV
PROTONS PARALLEL
TO SPIN VECTOR
NUMBER FLUX = 100
BKGD
ENERGY FLUX IN EV/ (CM2 SEC SR EV)
ENERGY IN EV
10^7
10^6
10^5
10^4
10^3
100
1000
10000

Figure 1

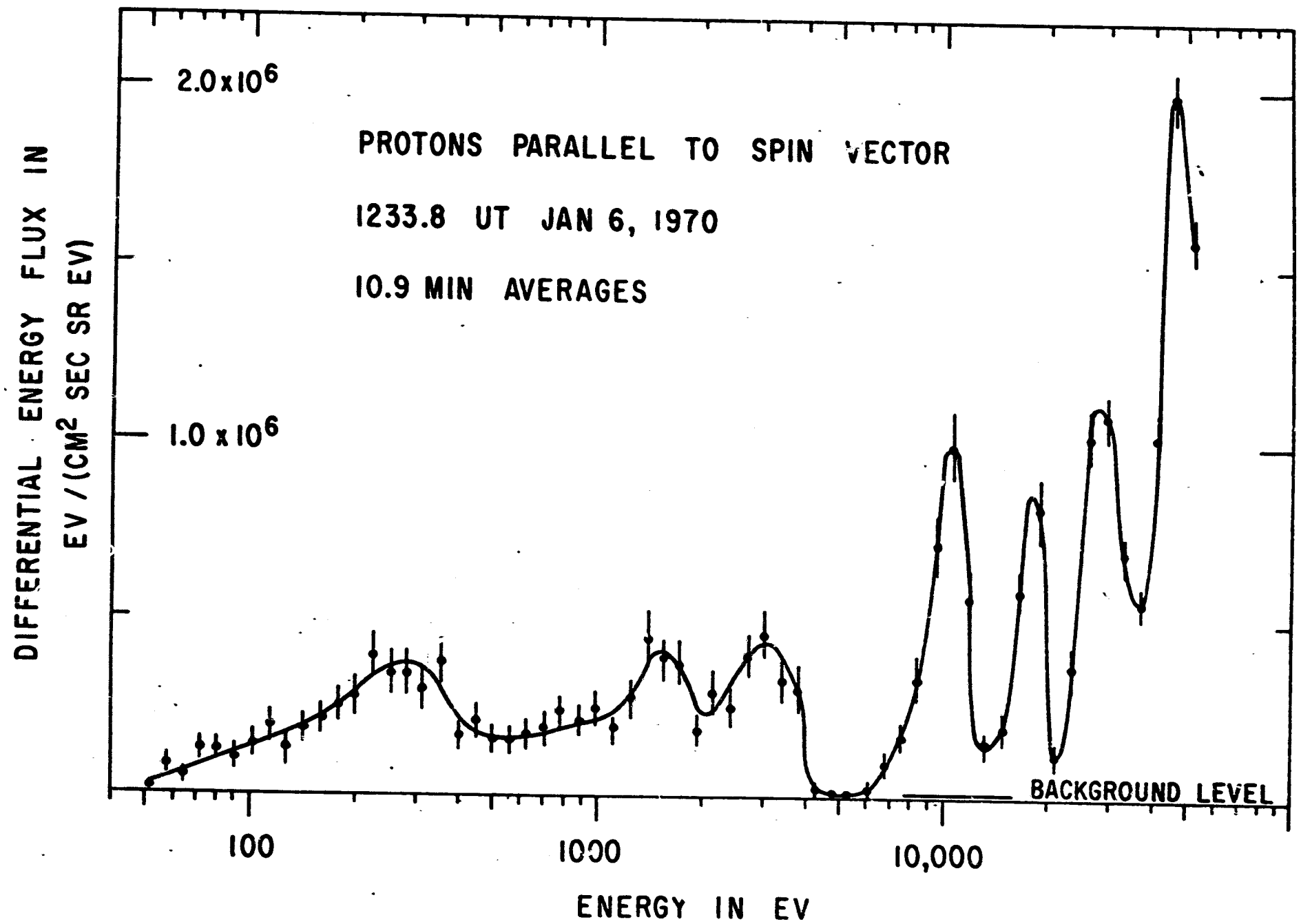
PROTONS PARALLEL TO SPIN VECTOR
1233.8 UT JAN 6, 1970
10.9 MIN AVERAGES
2.0x10^6
1.0 x10^6
DIFFERENTIAL ENERGY FLUX IN
EV /(CM^2 SEC SR EV)
BACKGROUND LEVEL
100
1000
10,000
ENERGY IN EV

Figure 2

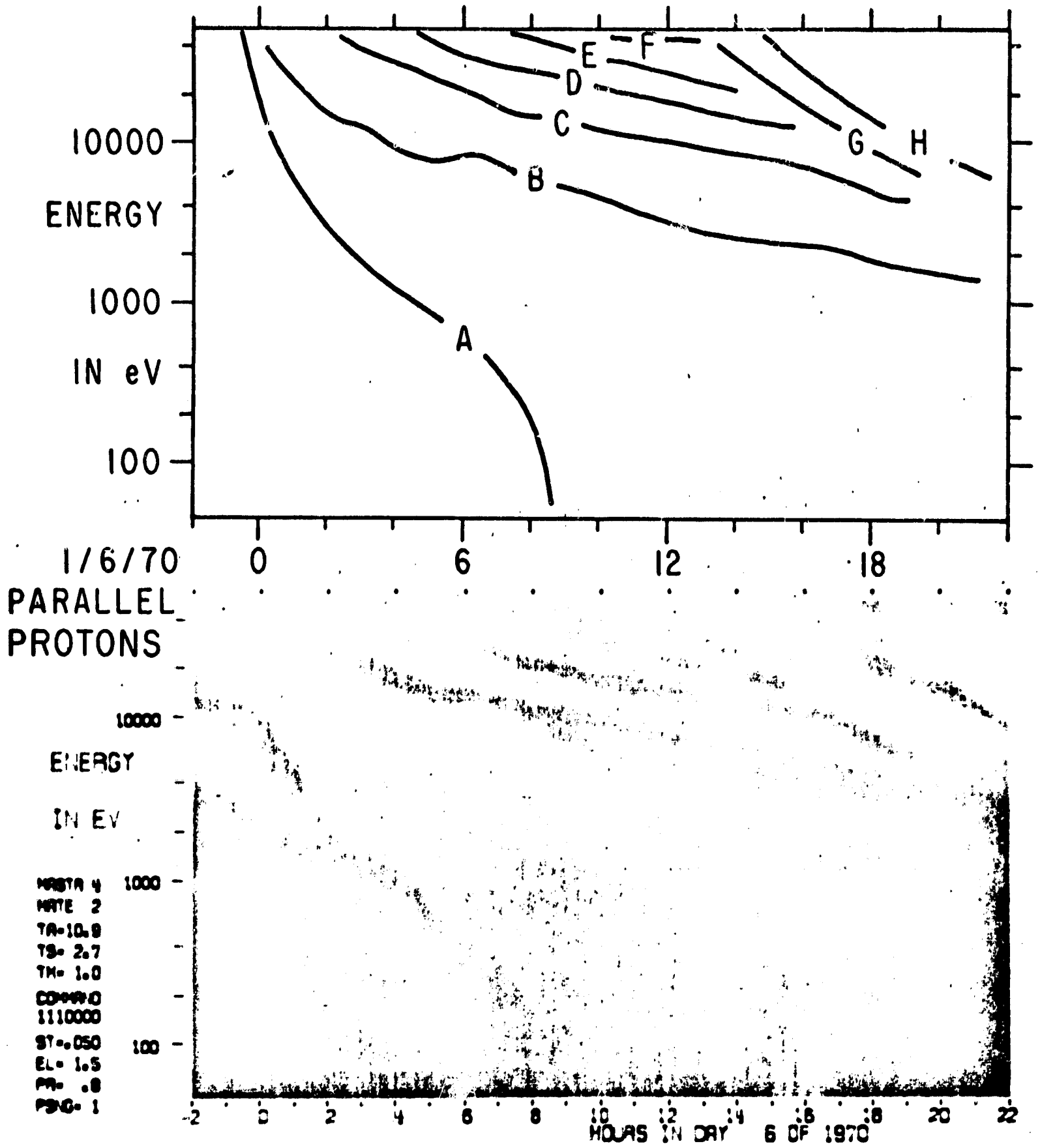
10000
ENERGY
1000
IN eV
100
A
B
C
D
E
F
G
H
1/6/70
0
6
12
18
PARALLEL
PROTONS
10000
ENERGY
IN EV
1000
100
-2
0
2
4
6
8
10
12
14
16
18
20
22
HOURS IN DAY 6 OF 1970

Figure 3

REPRODUCIBILITY OF THE ORIGINAL PAGE IS POOR.

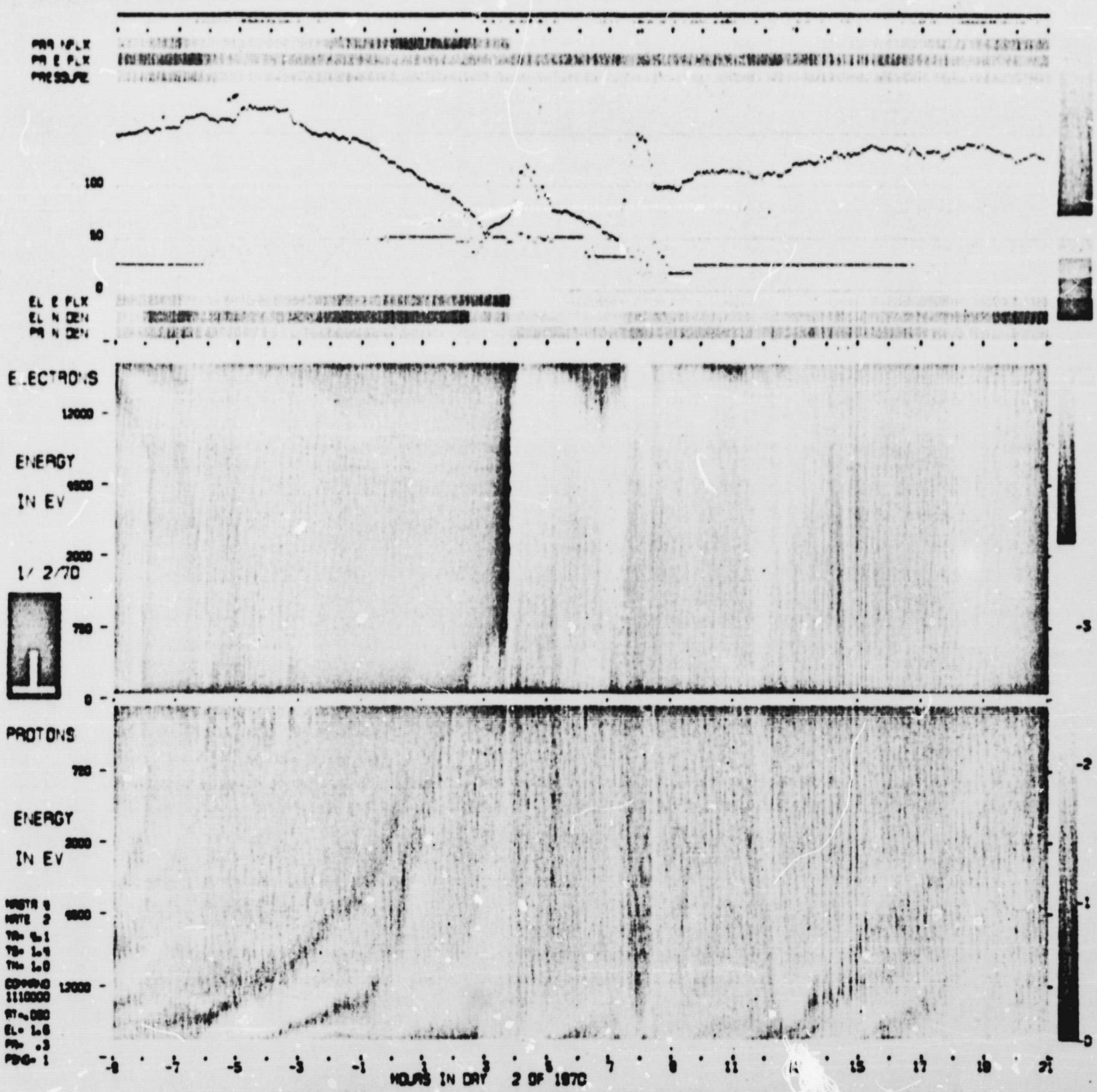

Figure 4

REPRODUCIBILITY OF THE ORIGINAL PAGE IS POOR.

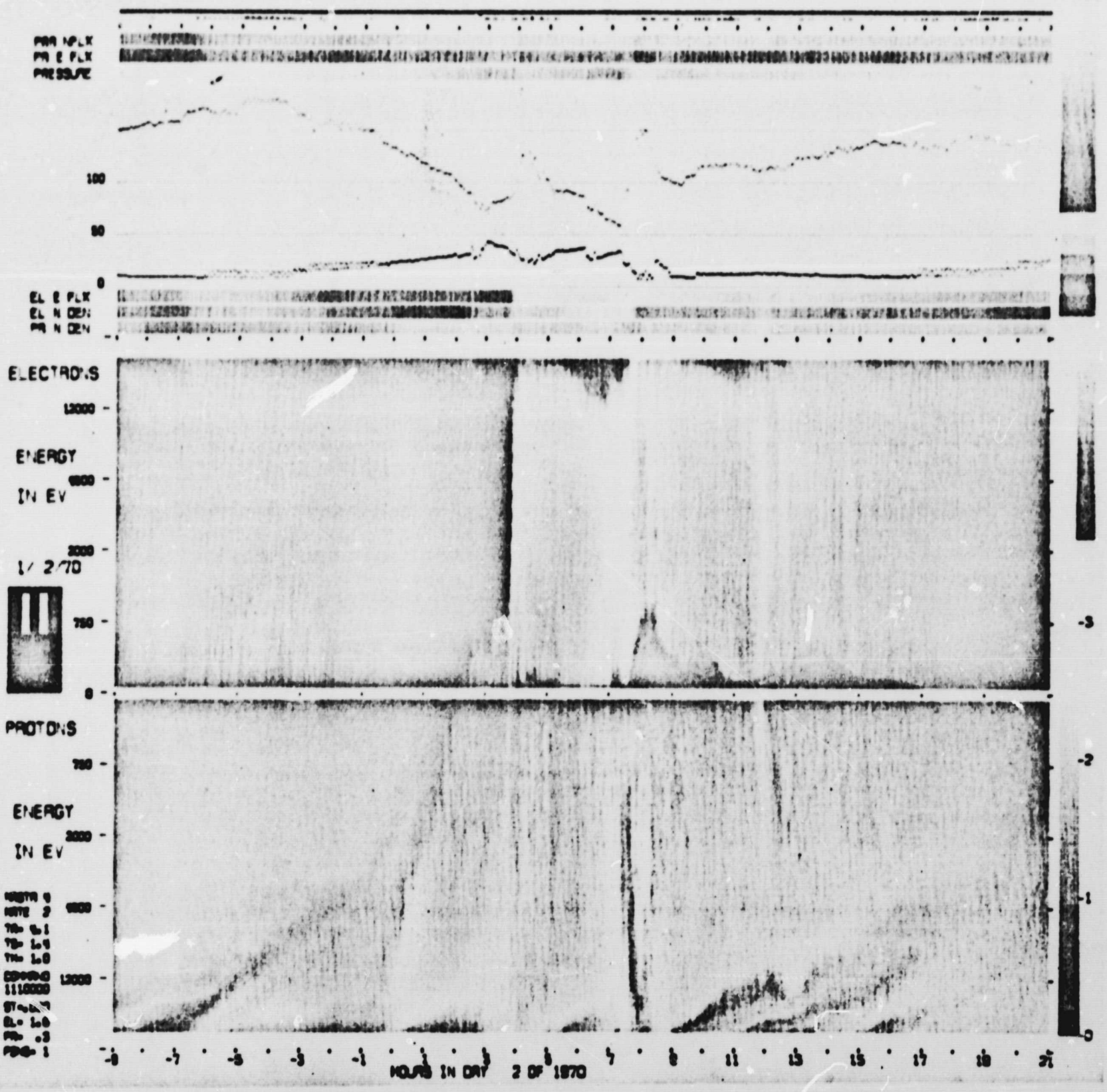

Figure 5

REPRODUCIBILITY OF THE ORIGINAL PAGE IS POOR.

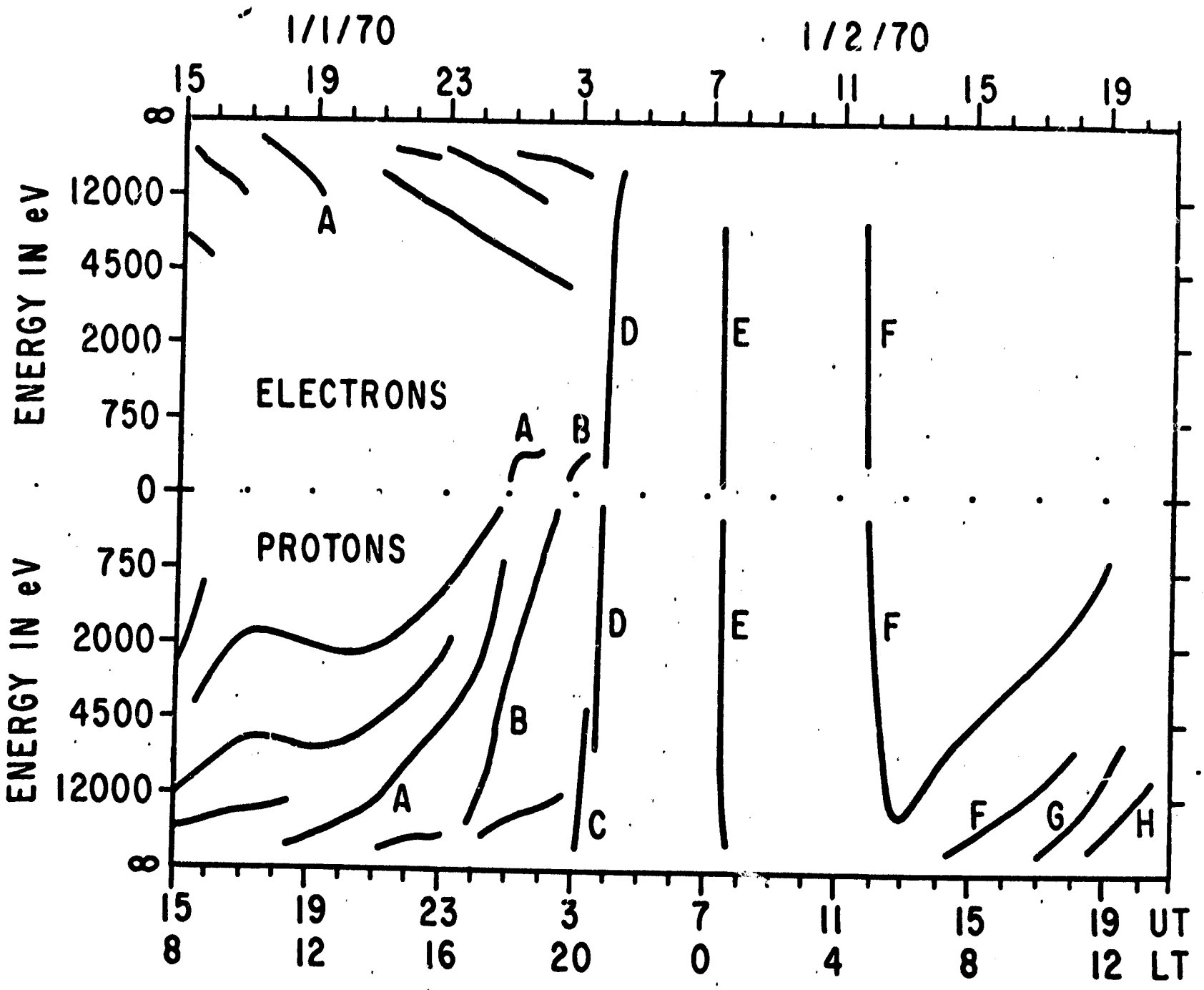

Figure 6

REPRODUCIBILITY OF THE ORIGINAL PAGE IS POOR.

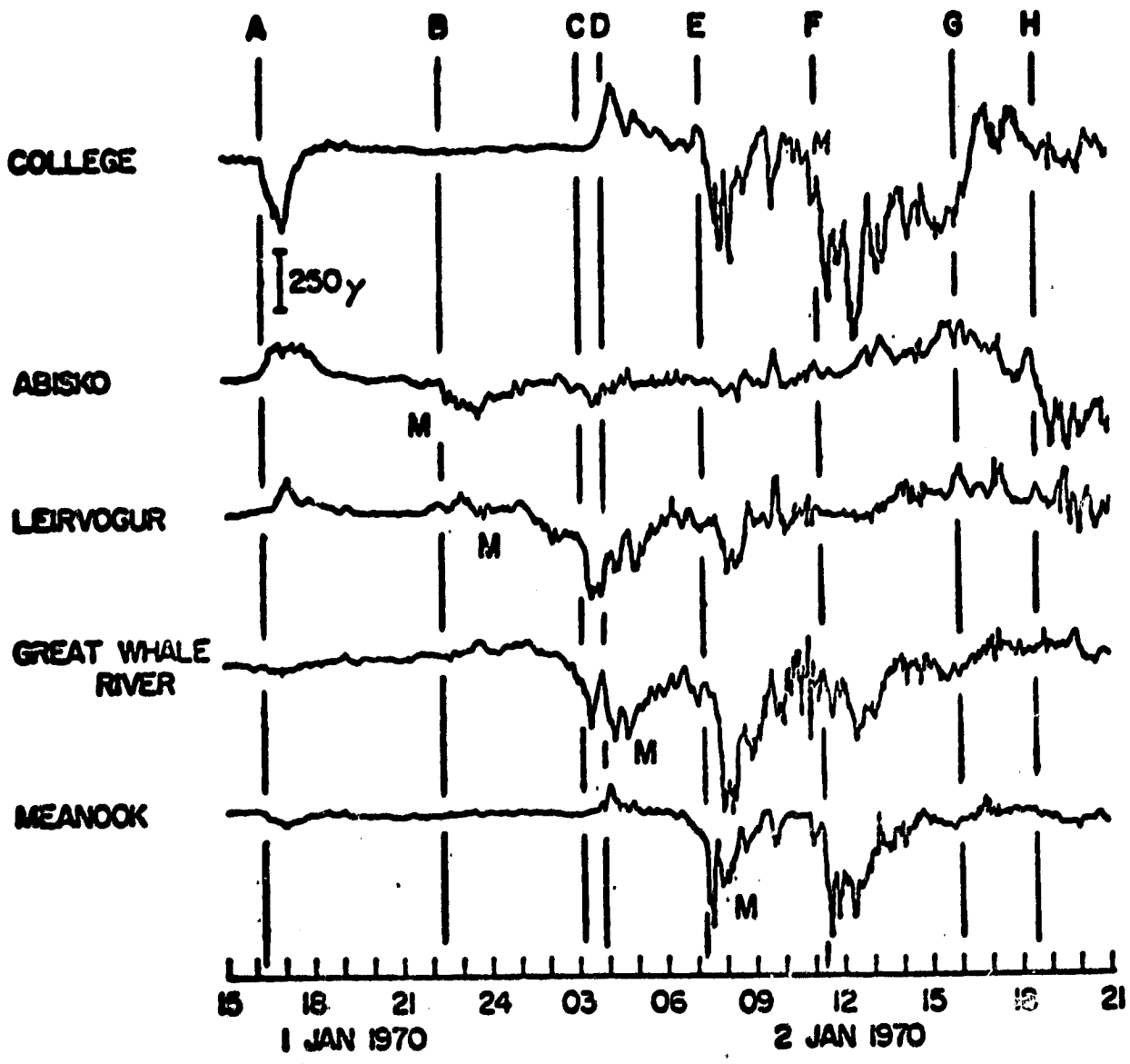

Figure 7

REPRODUCIBILITY OF THE ORIGINAL PAGE IS POOR.

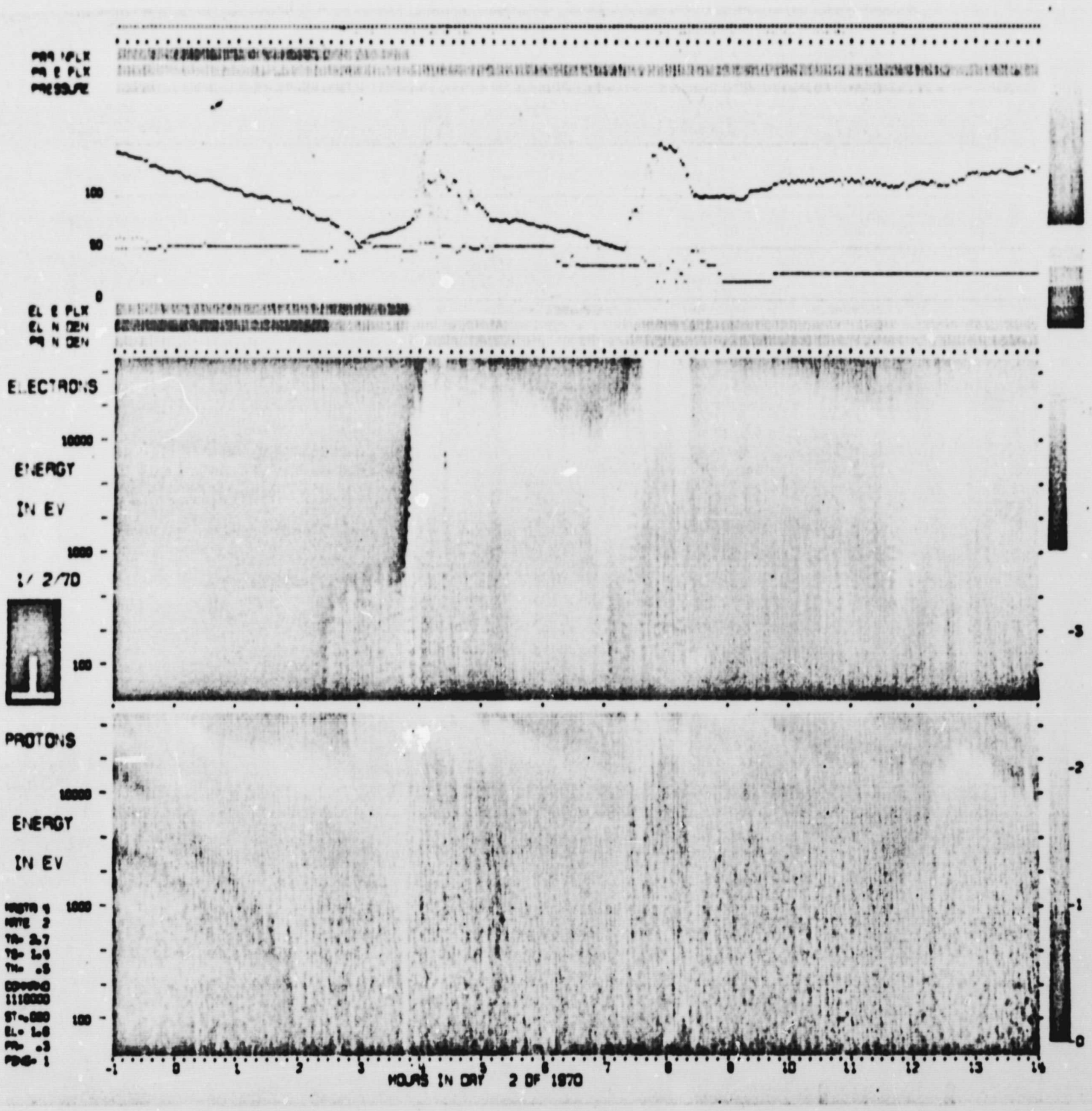

Figure 8

REPRODUCIBILITY OF THE ORIGINAL PAGE IS POOR.

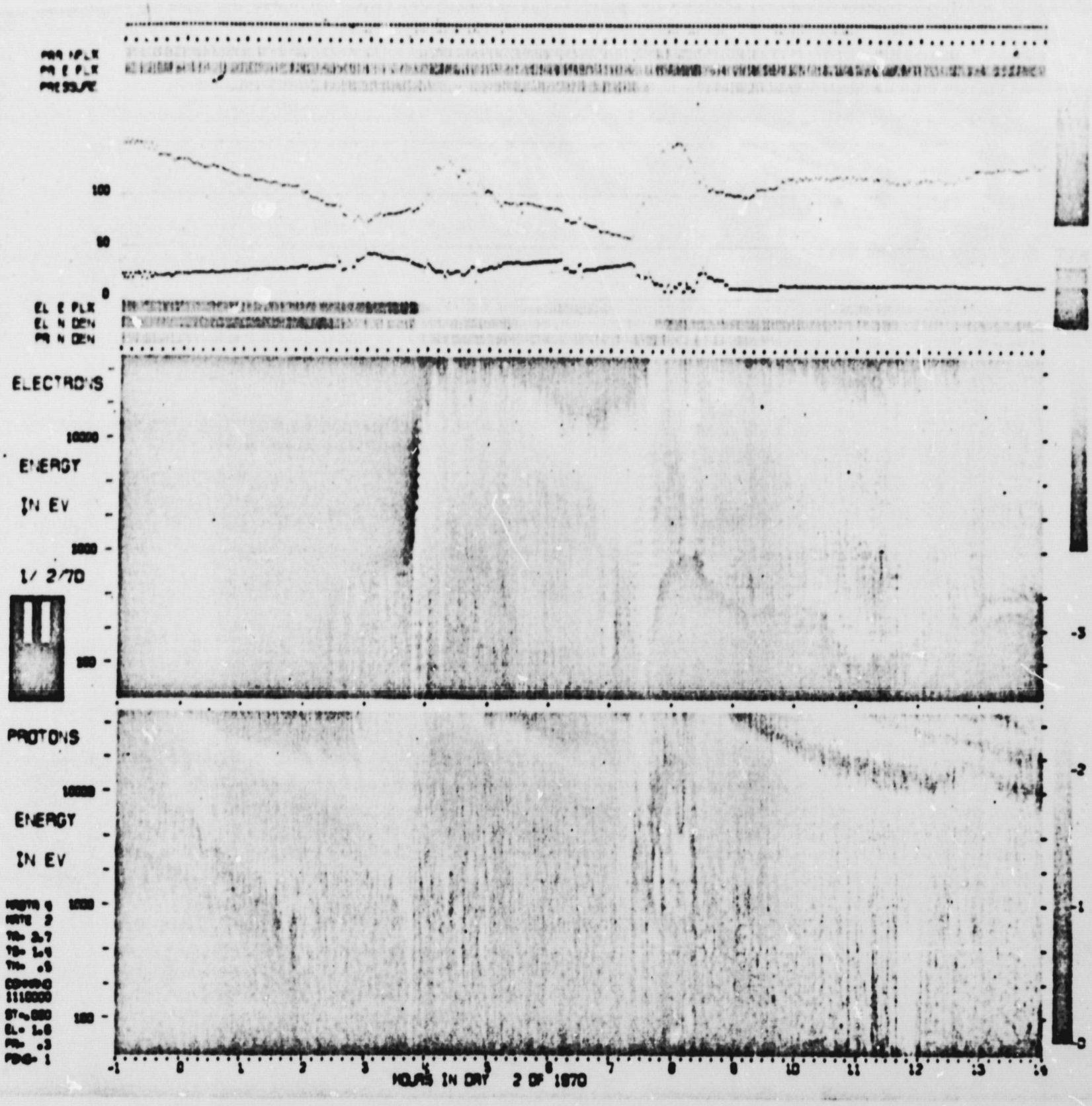

Figure 9

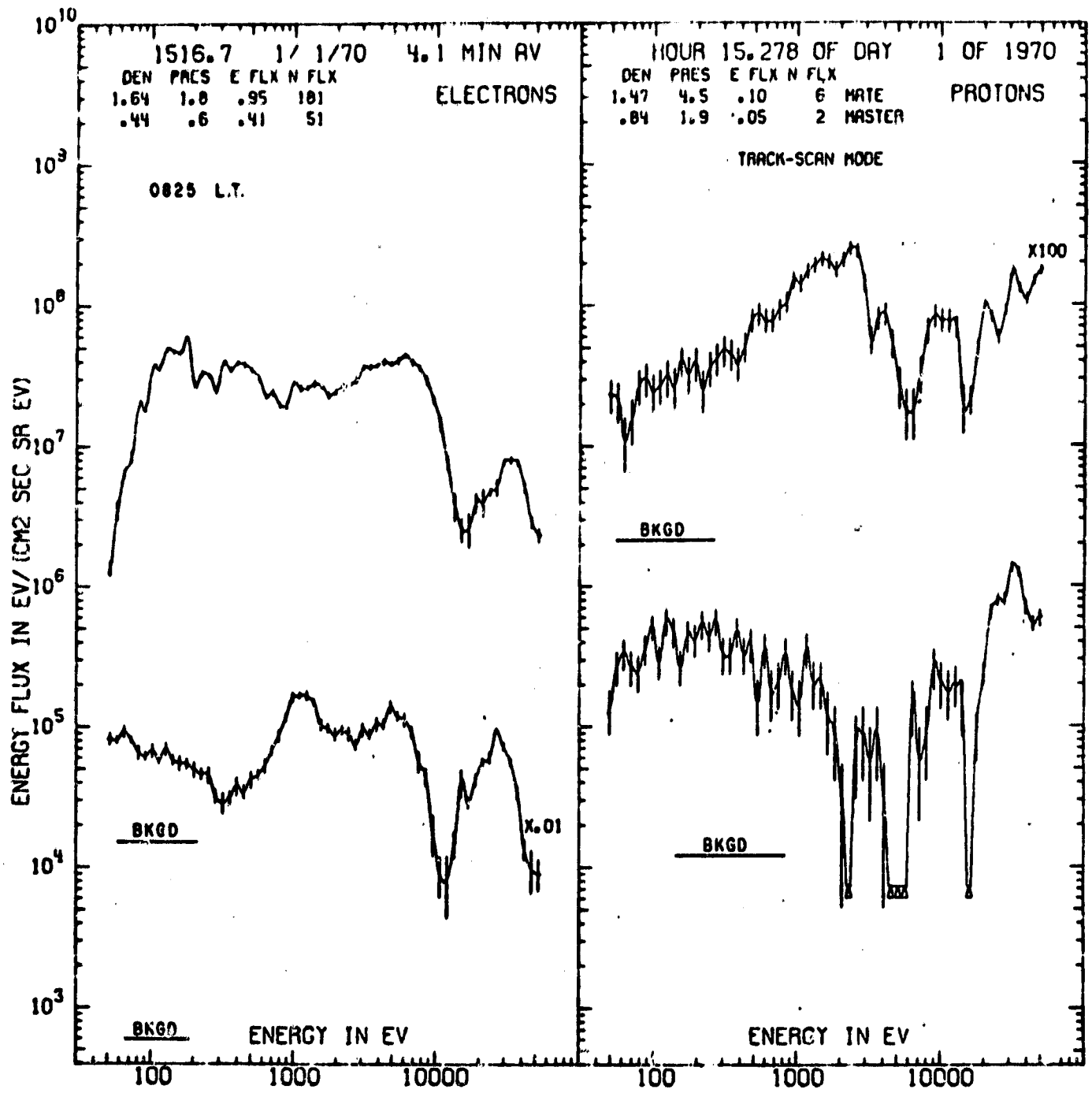
1516.7 1/ 1/70 4.1 MIN AV
DEN PRES E FLX N FLX
1.64 1.8 .95 181
.44 .6 .41 51
ELECTRONS
0825 L.T.
BKGD
X.01
BKGD
ENERGY IN EV
HOUR 15.278 OF DAY 1 OF 1970
DEN PRES E FLX N FLX
1.47 4.5 .10 6 MATE
.84 1.9 .05 2 MASTER
PROTONS
TRACK-SCAN MODE
X100
BKGD
BKGD
ENERGY IN EV
ENERGY FLUX IN EV/(CM2 SEC SR EV)
100
1000
10000

Figure 10

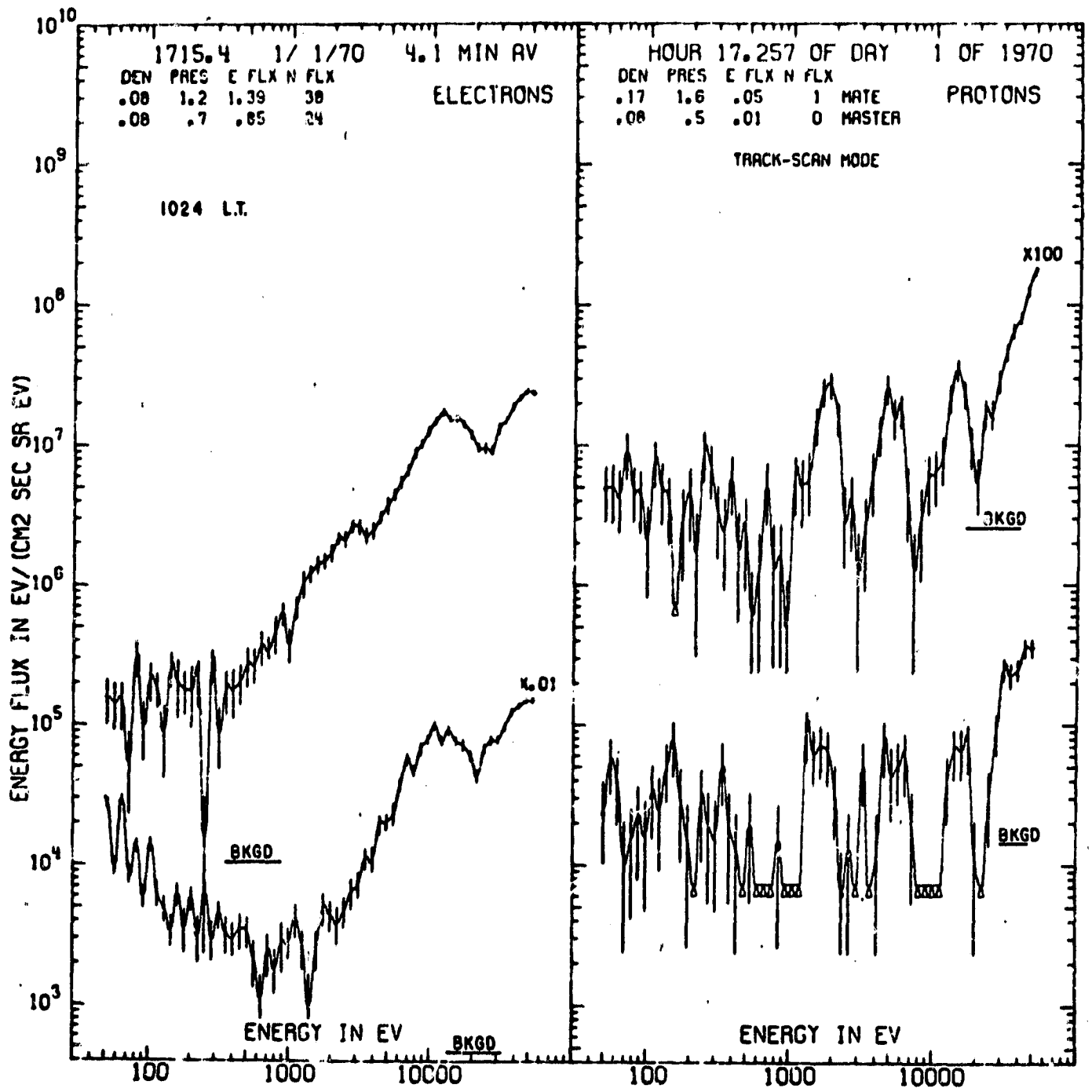
1715.4 1/ 1/70 4.1 MIN AV
DEN PRES E FLX N FLX
.08 1.2 1.39 38
.08 .7 .85 24
ELECTRONS
1024 L.T.
BKGD
x.01
ENERGY IN EV
BKGD
HOUR 17.257 OF DAY 1 OF 1970
DEN PRES E FLX N FLX
.17 1.6 .05 1 MATE
.08 .5 .01 0 MASTER
PROTONS
TRACK-SCAN MODE
X100
BKGD
BKGD
ENERGY IN EV
ENERGY FLUX IN EV/(CM2 SEC SR EV)
100
1000
10000

Figure 11

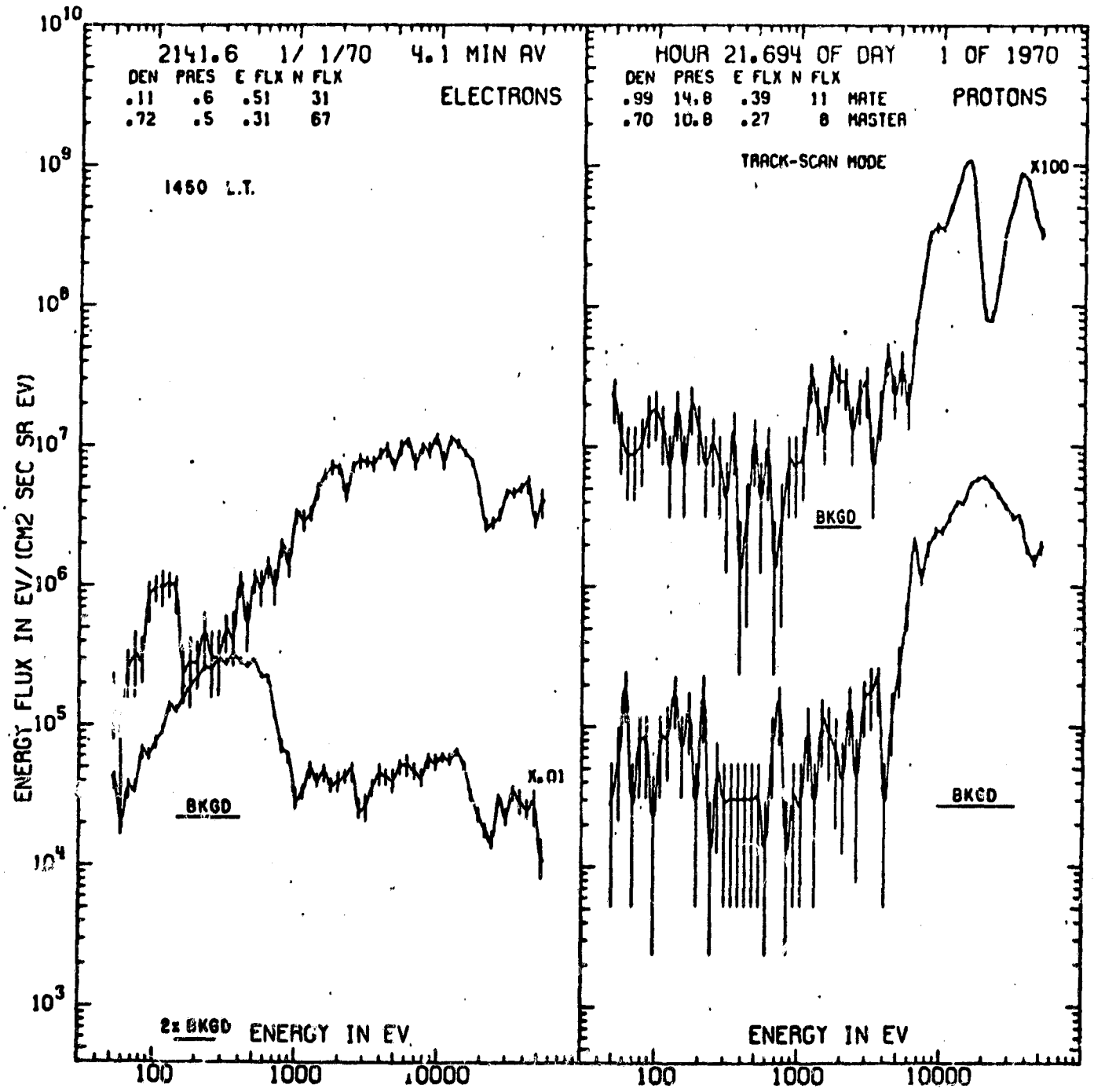
2141.6 1/ 1/70 4.1 MIN AV
DEN PRES E FLX N FLX
.11 .6 .51 31
.72 .5 .31 67
ELECTRONS
1450 L.T.
BKGD
X.01
2x BKGD
ENERGY IN EV
HOUR 21.694 OF DAY 1 OF 1970
DEN PRES E FLX N FLX
.99 14.8 .39 11 MATE
.70 10.8 .27 8 MASTER
PROTONS
TRACK-SCAN MODE
X100
BKGD
BKGD
ENERGY IN EV
ENERGY FLUX IN EV/(CM2 SEC SR EV)
100
1000
10000

Figure 12

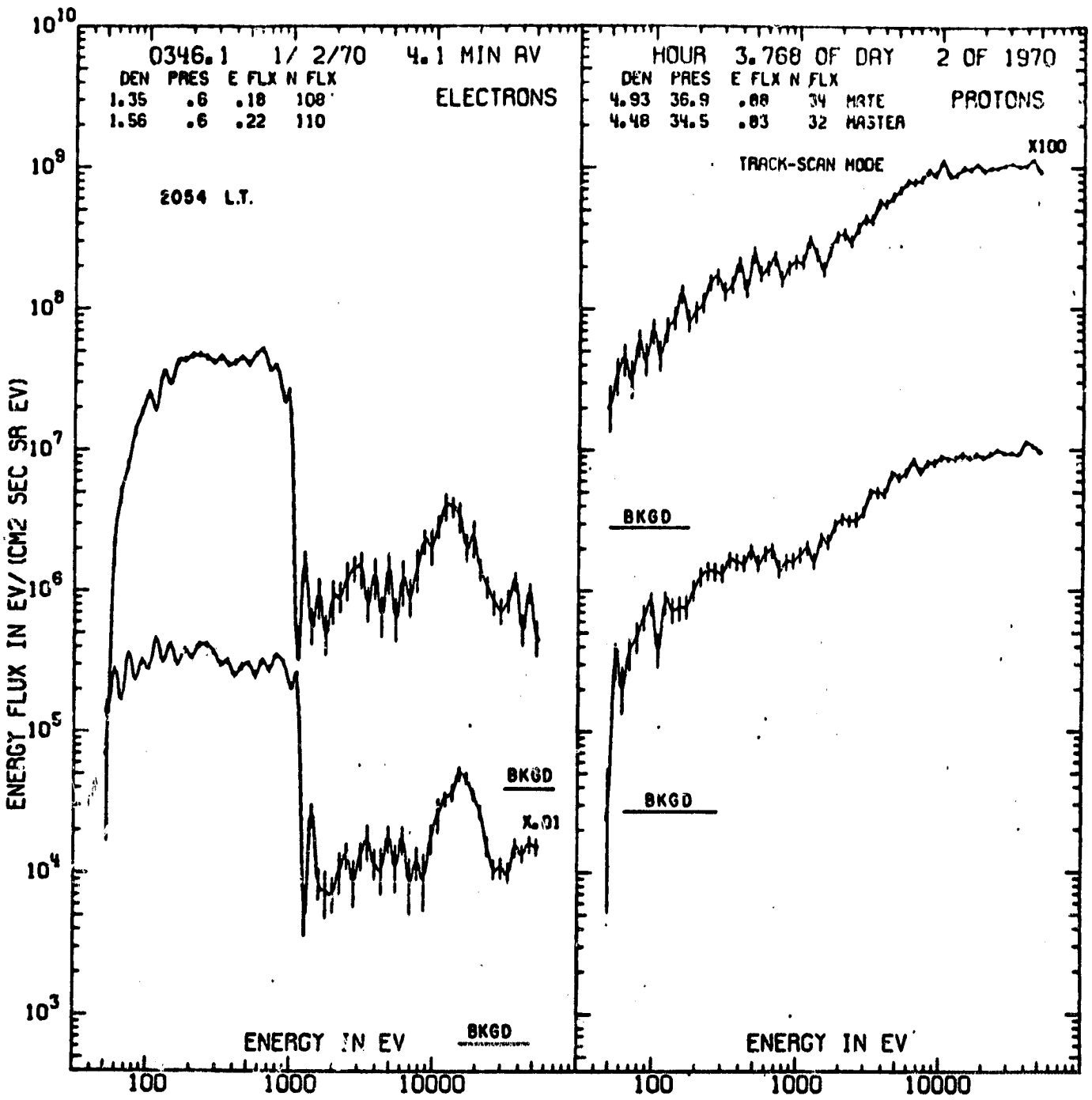
0346.1 1/ 2/70 4.1 MIN AV
DEN PRES E FLX N FLX
1.35 .6 .18 108
1.56 .6 .22 110
ELECTRONS
2054 L.T.
BKGD
X.01
BKGD
ENERGY IN EV
ENERGY FLUX IN EV/(CM2 SEC SR EV)
HOUR 3.768 OF DAY 2 OF 1970
DEN PRES E FLX N FLX
4.93 36.9 .08 34 MATE
4.48 34.5 .03 32 MASTER
PROTONS
TRACK-SCAN MODE
X100
BKGD
BKGD
ENERGY IN EV

Figure 13

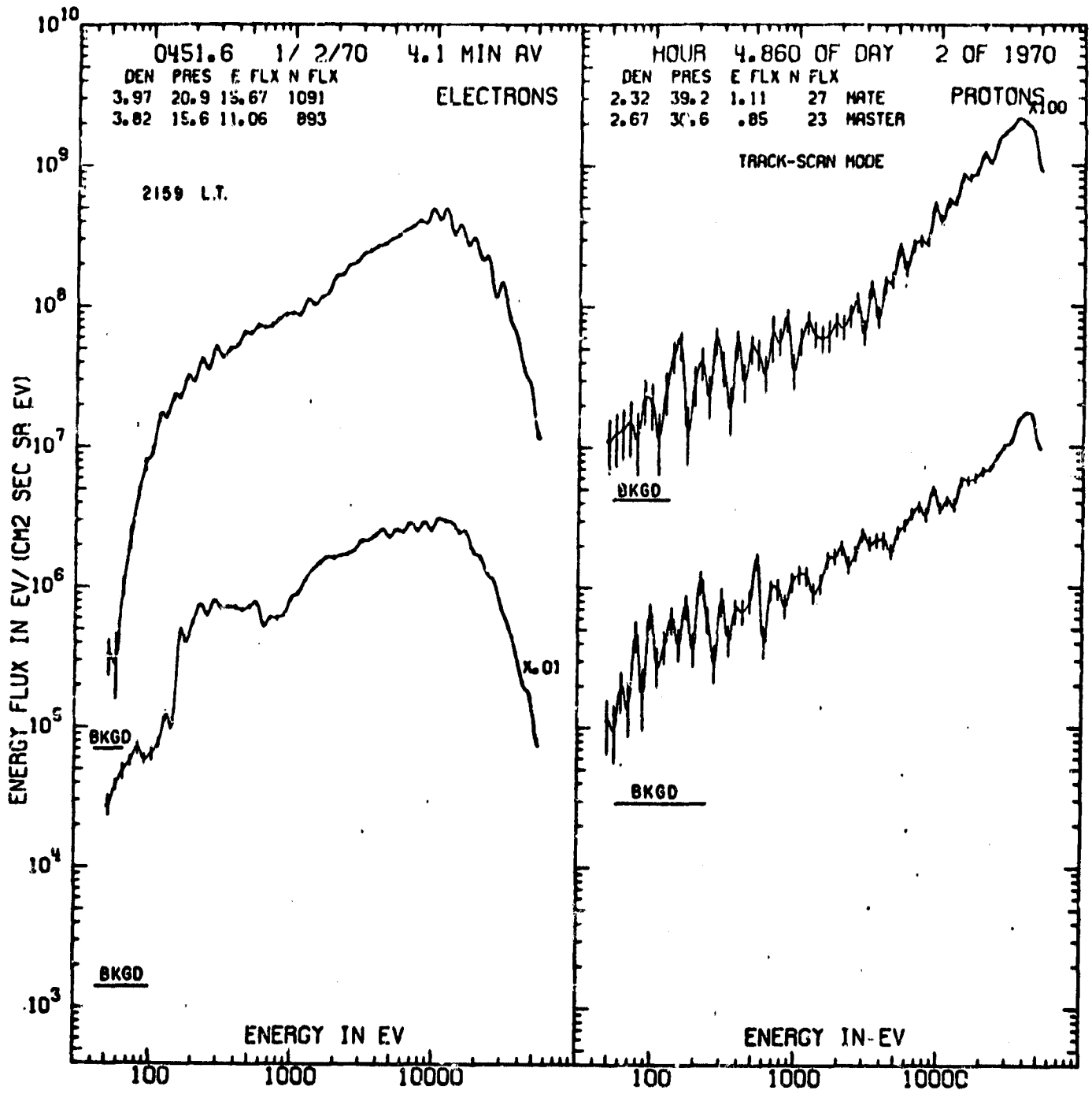
0451.6 1/ 2/70 4.1 MIN AV
DEN PRES E FLX N FLX
3.97 20.9 15.67 1091
3.82 15.6 11.06 893
ELECTRONS
2159 L.T.
BKGD
BKGD
x.01
ENERGY FLUX IN EV/(CM2 SEC SR EV)
ENERGY IN EV
HOUR 4.860 OF DAY 2 OF 1970
DEN PRES E FLX N FLX
2.32 39.2 1.11 27 MATE
2.67 30.6 .85 23 MASTER
PROTONS
x100
TRACK-SCAN MODE
BKGD
BKGD
ENERGY IN-EV

Figure 14

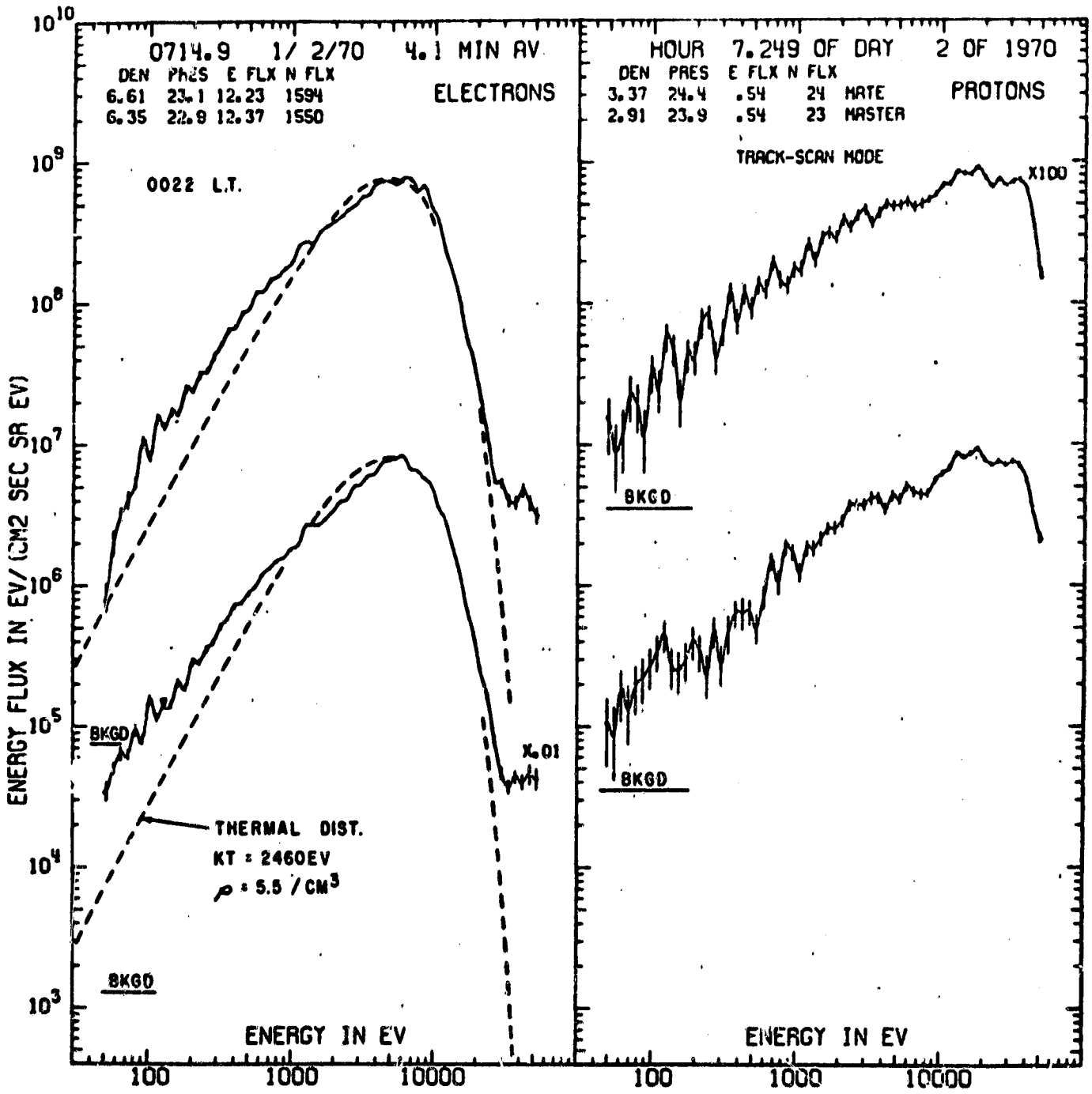
0714.9 1/ 2/70 4.1 MIN AV
DEN PRES E FLX N FLX
6.61 23.1 12.23 1594
6.35 22.9 12.37 1550
ELECTRONS
0022 L.T.
BKGD
X.01
THERMAL DIST.
KT = 2460EV
ρ = 5.5 /CM3
ENERGY FLUX IN EV/(CM2 SEC SR EV)
ENERGY IN EV
HOUR 7.249 OF DAY 2 OF 1970
DEN PRES E FLX N FLX
3.37 24.4 .54 24 MATE
2.91 23.9 .54 23 MASTER
PROTONS
TRACK-SCAN MODE
X100
BKGD
BKGD
ENERGY IN EV

Figure 15

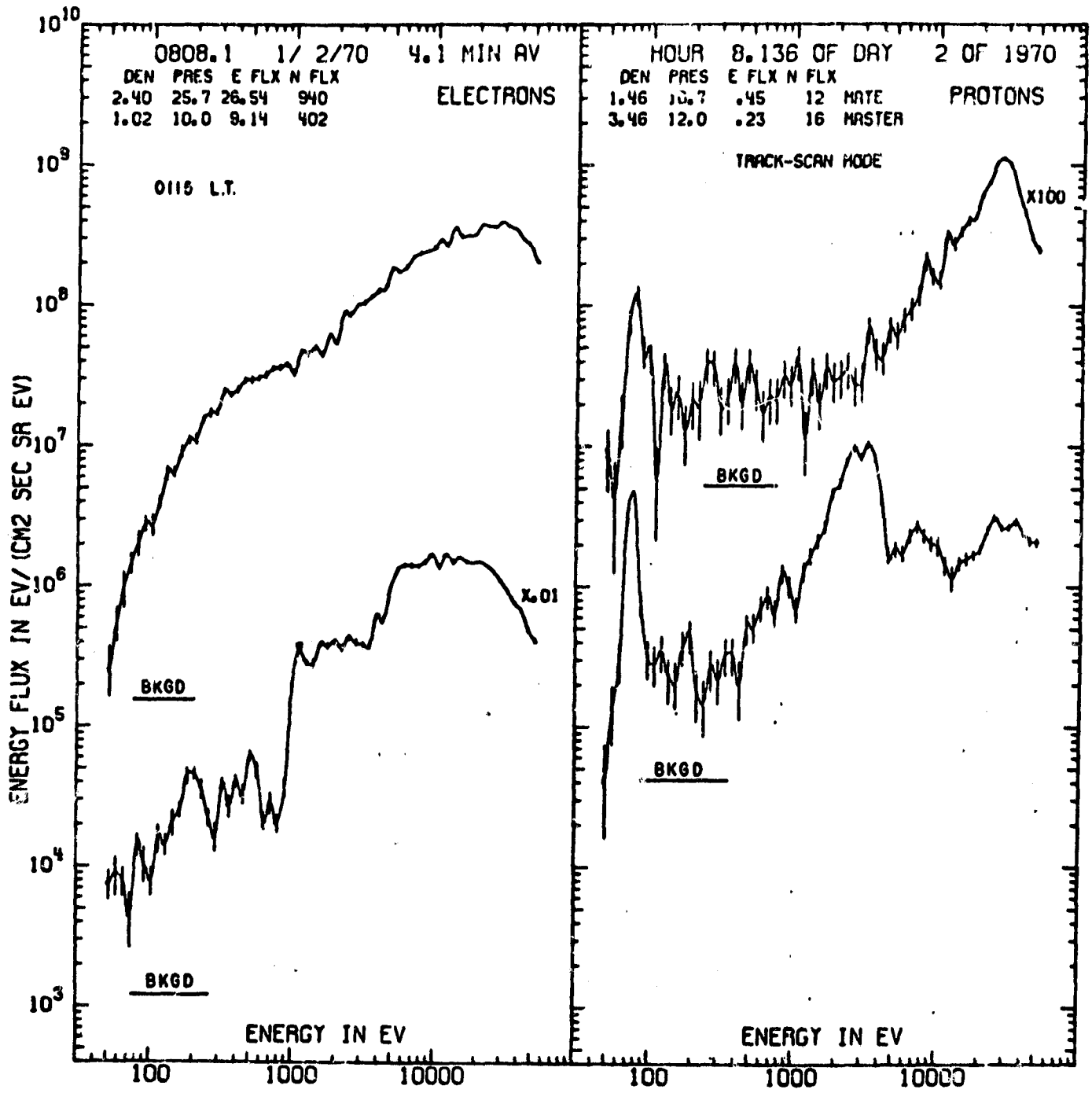
0808.1 1/ 2/70 4.1 MIN AV
DEN PRES E FLX N FLX
2.40 25.7 26.54 940
1.02 10.0 9.14 402
ELECTRONS
0115 L.T.
BKGD
X.01
BKGD
ENERGY IN EV
HOUR 8.136 OF DAY 2 OF 1970
DEN PRES E FLX N FLX
1.46 .45 12 MATE
3.46 12.0 .23 16 MASTER
PROTONS
TRACK-SCAN MODE
X100
BKGD
BKGD
ENERGY IN EV
ENERGY FLUX IN EV/(CM2 SEC SR EV)
100
1000
10000

Figure 16

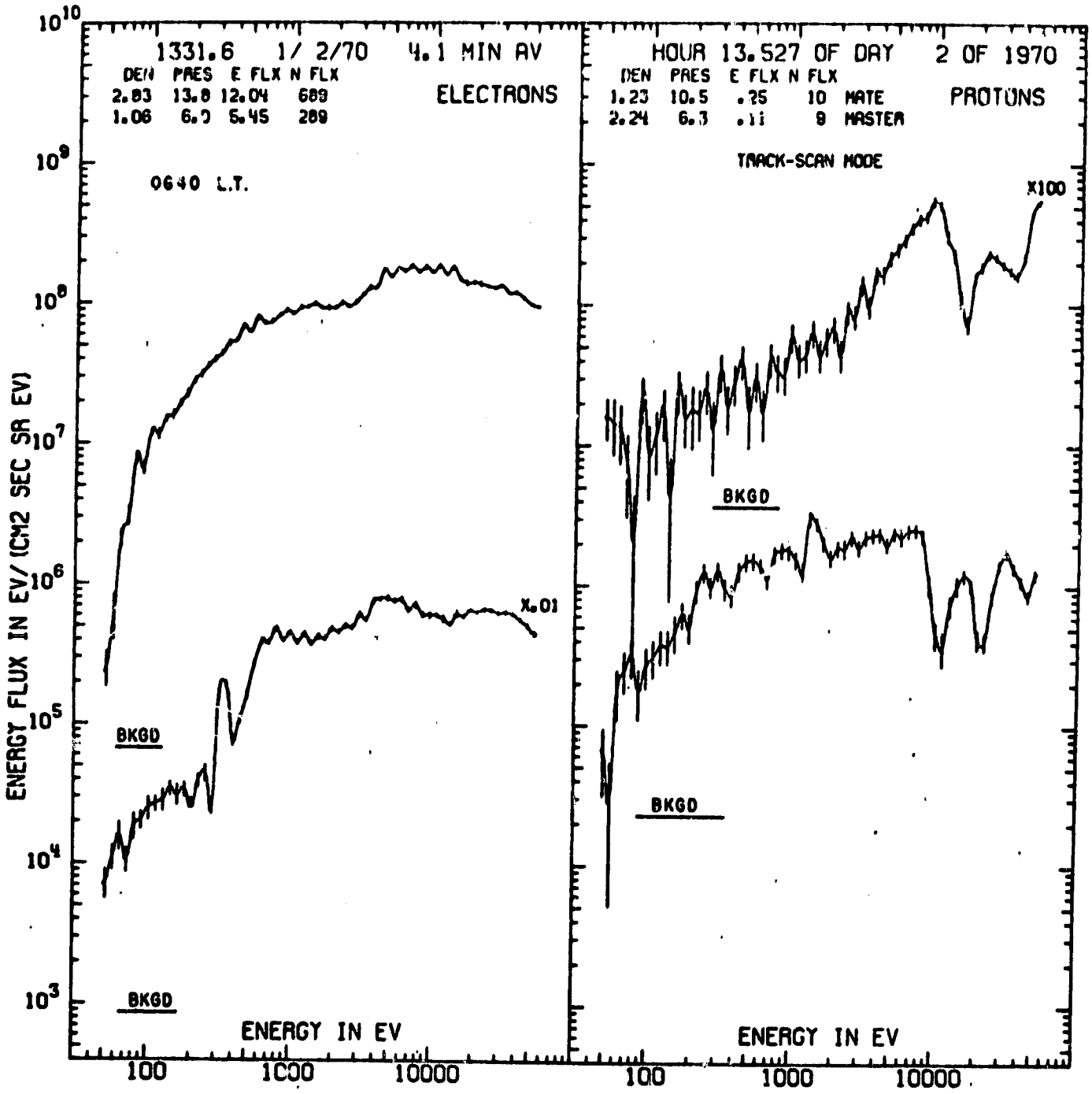
1331.6 1/ 2/70 4.1 MIN AV
DEN PRES E FLX N FLX
2.83 13.8 12.04 689
1.06 6.0 5.45 289
ELECTRONS
0640 L.T.
BKGD
X.01
BKGD
ENERGY IN EV
100
1000
10000
HOUR 13.527 OF DAY 2 OF 1970
DEN PRES E FLX N FLX
1.23 10.5 .25 10 MATE
2.24 6.3 .11 8 MASTER
PROTONS
TRACK-SCAN MODE
X100
BKGD
BKGD
ENERGY IN EV
100
1000
10000
ENERGY FLUX IN EV/(CM2 SEC SR EV)
10^{10}
10^{9}
10^{8}
10^{7}
10^{6}
10^{5}
10^{4}
10^{3}

Figure 17

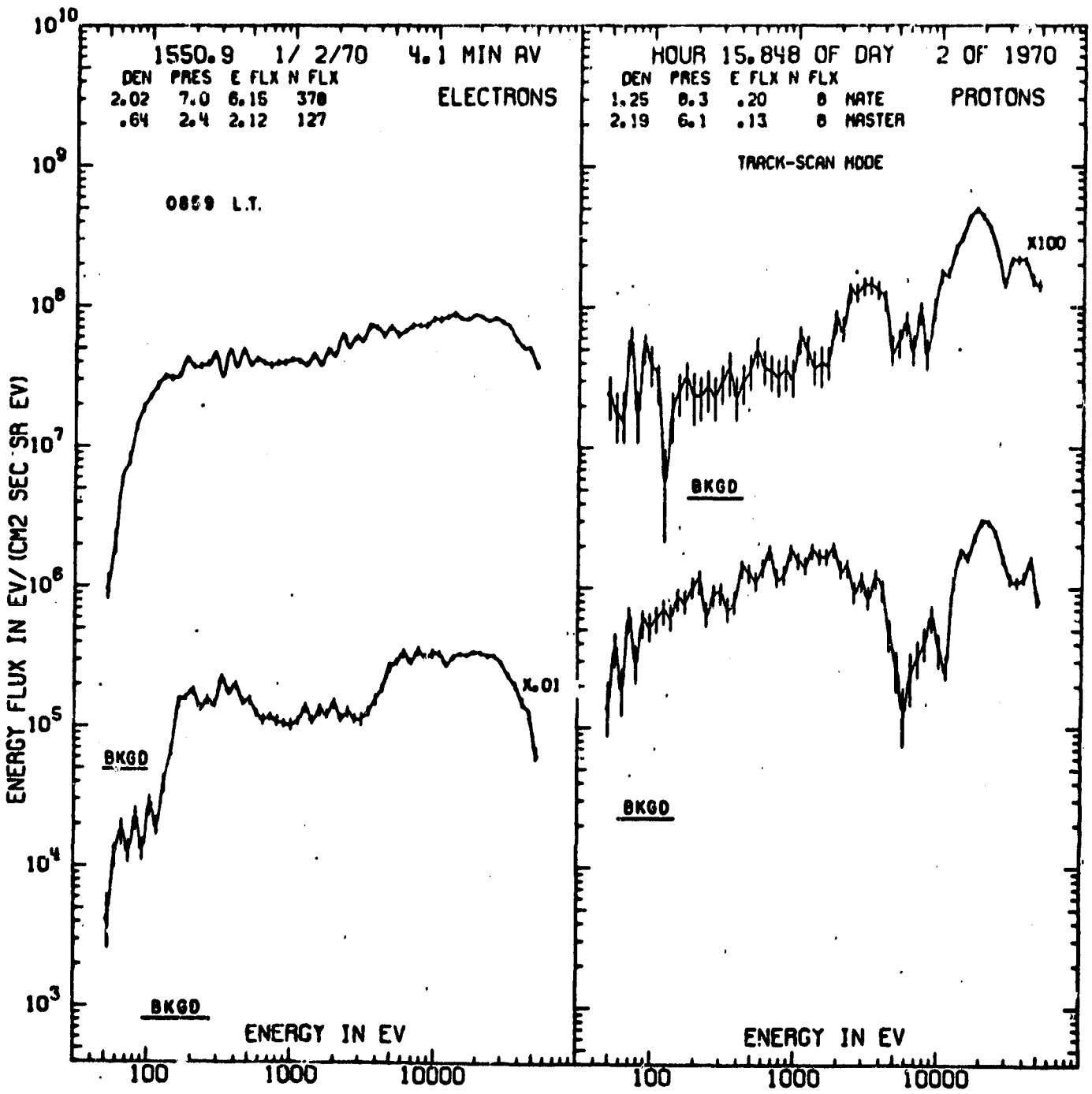
1550.9 1/ 2/70 4.1 MIN AV
DEN PRES E FLX N FLX
2.02 7.0 6.15 378
.64 2.4 2.12 127
ELECTRONS
0859 L.T.
BKGD
X.01
BKGD
ENERGY IN EV
HOUR 15.848 OF DAY 2 OF 1970
DEN PRES E FLX N FLX
1.25 8.3 .20 8 NATE
2.19 6.1 .13 8 NASTER
PROTONS
TRACK-SCAN MODE
X100
BKGD
BKGD
ENERGY IN EV
ENERGY FLUX IN EV/(CM2 SEC SR EV)
100
1000
10000

Figure 18

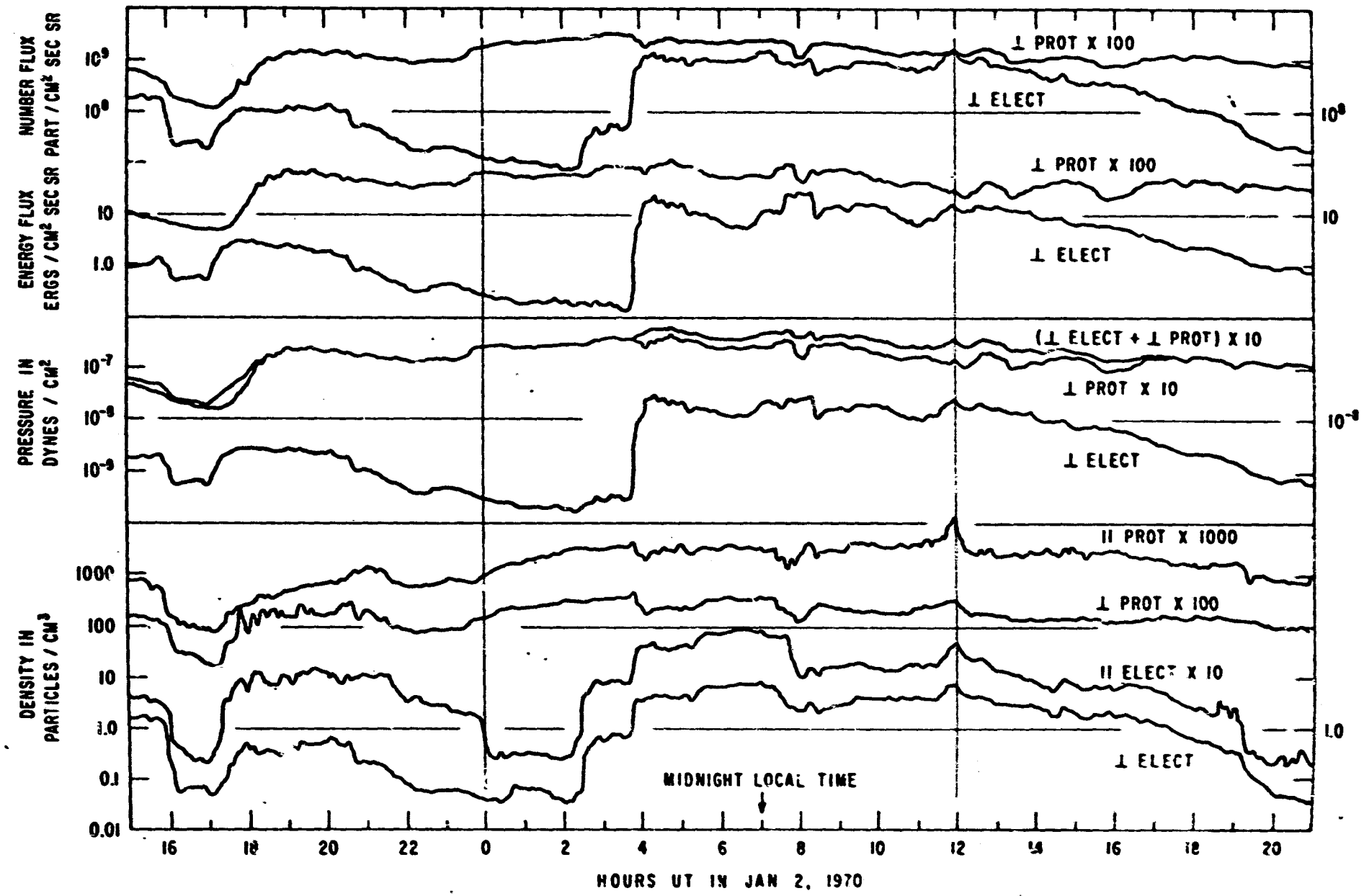
NUMBER FLUX
PART / CM² SEC SR
ENERGY FLUX
ERGS / CM² SEC SR
PRESSURE IN
DYNES / CM²
DENSITY IN
PARTICLES / CM³
⊥ PROT X 100
⊥ ELECT
⊥ PROT X 100
⊥ ELECT
(⊥ ELECT + ⊥ PROT) X 10
⊥ PROT X 10
⊥ ELECT
∥ PROT X 1000
⊥ PROT X 100
∥ ELECT X 10
⊥ ELECT
MIDNIGHT LOCAL TIME
HOURS UT IN JAN 2, 1970

Figure 19